[26]R. L. Bramblett, J. T. Caldwell, B. L. Berman, R. R. Harvey, and S. C. Fultz, Phys. Rev. 148, 1198 (1966).
[27]P. H. Stelson and L. Grodzins, Nucl. Data A1, 29 (1965).
[28]R. H. Hofstadter, Rev. Mod. Phys. 28, 214 (1956).
[29]B. Block and H. Feshbach, Ann. Phys. (N.Y.) 23, 47 (1963); H. Feshbach, A. K. Kerman, and R. H. Lemmer, *ibid.* 41, 230 (1967).
[30]C. E. Porter and R. G. Thomas, Phys. Rev. 104, 483 (1956).
[31]L. Wilets, *Theories of Nuclear Fission* (Clarendon Press, University of Oxford, Oxford, England, 1964).
[32]B. L. Berman, R. J. Baglan, and C. D. Bowman, Phys. Rev. Letters 24, 319 (1970).
[33]S. Fallieros, B. Goulard, and R. H. Ventner, Phys. Letters 19, 389 (1965).
[34]J. S. O'Connell, B. F. Gibson, and E. Hayward, private communication.

PHYSICAL REVIEW C VOLUME 4, NUMBER 1 JULY 1971

Nuclear Structure of ^{22}Na: The ^{21}Ne(^{3}He,d) Reaction*

J. D. Garrett, R. Middleton, and H. T. Fortune
Physics Department, University of Pennsylvania, Philadelphia, Pennsylvania 19104

(Received 19 February 1971)

The bound states of ^{22}Na have been studied using the ^{21}Ne(^{3}He,d)^{22}Na reaction at a bombarding energy of 18 MeV. Angular distributions of the deuterons have been compared with distorted-wave Born-approximation predictions. The resulting spectroscopic factors are compared with those calculated using the rotational and shell models. (^{3}He,d) spectroscopic factors for $T=1$ final states in ^{22}Na are compared with (d,p) spectroscopic factors from a ^{21}Ne(d,p)^{22}Ne study. The levels of ^{22}Na are discussed in terms of Nilsson configurations and associated rotational bands.

I. INTRODUCTION

^{22}Na is an example of a deformed, odd-odd nucleus. Recent studies indicate that the nuclei in the region of mass 20–24 are among the most deformed nuclei known.[1-5] The rotational model has had considerable success in describing the collective properties of the odd-A and even-even nuclei near mass 22.[6-11] In this model, ^{22}Na is described as a proton and a neutron moving in a prolate deformed potential created by the remaining core nucleons. The low-lying states of ^{22}Na should then correspond to placing the odd proton and neutron in the lowest available Nilsson orbital,[12,13] $\Omega^\pi = \frac{3}{2}^+$, $[Nn_z\Lambda] = [211]$. The energy separation of the resulting 3^+ (ground state) and 0^+ ($E_x = 0.657$ MeV) states have been explained[14,15] in terms of the residual neutron-proton interaction and the Nilsson model. The low-lying states in ^{22}Na have been described as rotational bands based on the $(\frac{3}{2}^+[211])^2$ Nilsson configuration.[1,2,16] A negative-parity band[2,16] has also been suggested. These bands are summarized in Table I.

Experimentally the energy levels of ^{22}Na up to 8 MeV were established by the ^{23}Na(^{3}He, α)^{22}Na and ^{24}Mg(d, α)^{22}Na reactions.[17] The spins, parities, and γ-ray branching ratios of the states of ^{22}Na below 4.2 MeV are known principally from γ-ray decay studies[2,16,18-23] and lifetime measurements.[20,21,23-28] Additional spin-parity assignments were recently made in a study of the ^{20}Ne(^{3}He, p) reaction.[1] The ^{23}Na(p, d) reaction,[29] the ^{23}Na(d, t) reaction,[30,31] and the ^{22}Ne(^{3}He, t) reaction[32] have also yielded information for some of the low-lying levels of ^{22}Na. The previously known spins and parities of ^{22}Na below 5.2 MeV are summarized in Fig. 1.

The single-nucleon stripping reaction has not been performed previously because of the difficulty in preparing a mass-21 target. The stable nucleus of mass 21, ^{21}Ne, is only present as 0.27% of natural Ne and has only recently become available in enrichments >50%. In the present study the ^{21}Ne(^{3}He, d)^{22}Na reaction was performed at an incident energy of 18 MeV using a target of 86.5% ^{21}Ne. The angular distributions of deuteron groups have been compared with distorted-wave Born-approximation (DWBA) predictions. The resulting experimental spectroscopic factors were then compared with predicted spectroscopic factors calculated using Nilsson model and shell-model wave functions.

II. EXPERIMENTAL PROCEDURE AND RESULTS

The ^{21}Ne(^{3}He, d)^{22}Na reaction was studied at an incident energy of 18 MeV using a ^{3}He beam from the University of Pennsylvania tandem Van de Graaff accelerator. Reaction products were momentum analyzed at 12 angles between $7\frac{1}{2}$ and 90°

(lab) using a multi-angle magnetic spectrograph. The deuterons were detected in 50-μm Ilford $K2$ nuclear emulsions which were covered with 10-mil Mylar to absorb the elastically scattered ^{3}He and the α particles from the ^{21}Ne(^{3}He, α) reaction. The target which was contained in a rotating gas cell[33] was 25.75 Torr (28.7 μg/cm^2) of Ne gas enriched to 86.5% in ^{21}Ne.

A deuteron momentum spectrum measured at a lab angle of $7\frac{1}{2}°$ is shown in Fig. 2. Reaction products resulting from target impurities are identified by the levels of the corresponding residual nucleus. Experimental angular distributions of the deuteron groups leading to 35 bound states of ^{22}Na are shown in Figs. 3–7. DWBA predictions based on the final-state configurations stated in the figure captions, are shown in Figs. 3–6. The error bars represent statistical errors and uncertainties in separation of closely spaced states. An error of 20%, due principally to uncertainties in gas-target pressure and beam-current integration, is assigned to the absolute cross-section scale.

III. ANALYSIS

The analysis of the angular distributions was performed using the DWBA code DWUCK.[34] For a single-particle stripping reaction, the experimental cross section $\sigma_{\exp}(\theta)$, is related to the theoretical single-particle cross section (calculated using code DWUCK), $\sigma_{nlj}(\theta)$, by the expression

$$\sigma_{\exp}(\theta) = NC^2 \frac{2J_f+1}{2J_i+1} \sum_{nlj} S_{nlj} \frac{\sigma_{nlj}(\theta)}{2j+1}, \qquad (1)$$

where

$$C = \langle T_i T_{z_i} t t_z | T_f T_{z_f} \rangle . \qquad (2)$$

Here, J, T, and T_z are the spin, isospin, and z component of isospin, respectively; i and f refer to the target and the residual nucleus, and n, l, j, t, and t_z are quantum numbers of the transferred particle. The normalization factor, N, includes the overlap of the incident- and exiting-particle wave functions. The spectroscopic factor, S_{nlj}, is a measure of the overlap of the target plus transferred particle and the final state of the residual nucleus. Since $\sigma_{nlj}(\theta)$ corresponds to the cross section for adding a nucleon to an empty orbital of quantum numbers, n, l, j, the factor $(2j+1)$ must be included in the denominator. In

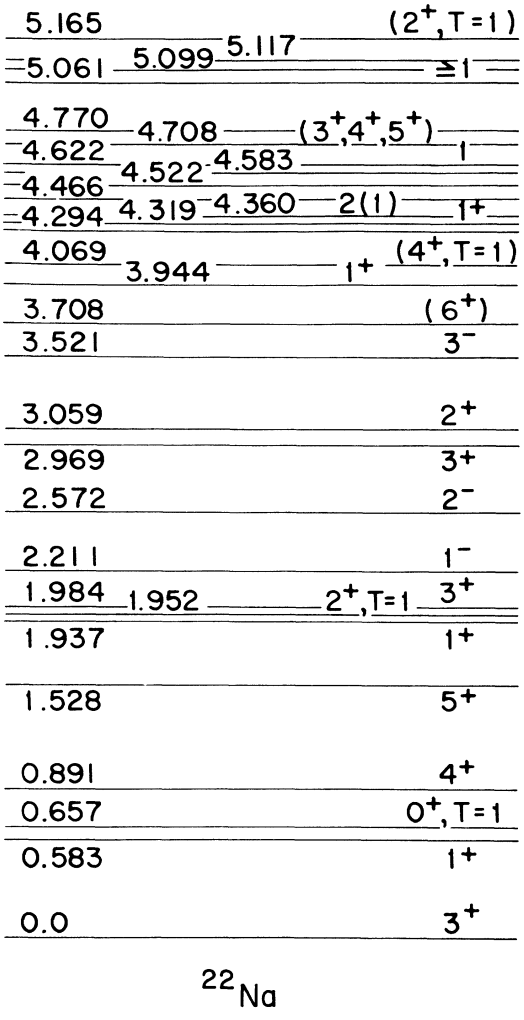

FIG. 1. Summary of the previously known spins and parities of the states of ^{22}Na below an excitation of 5.2 MeV. The spin and parity assignments are from the existing literature as summarized in the text.

TABLE I. Previously known rotational bands of ^{22}Na (see Refs. 1, 2, and 16).

Configuration	$(\frac{3}{2}^+[211])^2$	$(\frac{3}{2}^+[211])^2$	$(\frac{3}{2}^+[211])^2$	$\frac{3}{2}^+[211]$, $\frac{1}{2}^-[101]$ [a]
K, T	3, 0	0, 0	0, 1	1, 0
States (MeV)	g.s. 3^+	0.583 1^+	0.657 0^+	2.211 1^-
	0.891 4^+	1.984 3^+	1.952 2^+	2.572 2^-
	1.528 5^+	[4.708 (5^+)]	4.069 $(4)^+$	3.521 3^-
	3.708 (6^+)			

[a] Though this band was previously suggested, its association with this configuration is from the present study.

the literature (and, e.g., in the DWBA code JULIE[35]), the single-particle cross section is often defined as an average rather than a sum over the magnetic quantum number m; hence the expression relating the theoretical single-particle cross section and the experimental cross section is written without the factor $(2j+1)$ in the denominator.

The appropriate elastic scattering measurements were not available to determine the entrance- and exit-channel optical-model parameters. However, for light, deformed nuclei (where a simple optical-model description of the elastic scattering is not valid) better results are usually obtained in DWBA calculations by using average optical-model parameters applicable to the given energy and mass region. The optical-model parameters used in the present analysis are listed in Table II. All the calculations were performed using a Thomas spin-orbit strength of $\lambda = 25$ in the bound state even though it is known[36] that this value may lead to a reduced theoretical cross section for $j = l - \frac{1}{2}$.

Figure 8 illustrates the effects of finite-range, nonlocal (FRNL) corrections on the DWBA calculations. Finite-range corrections were applied using the method of Buttle and Goldfarb[37] and a finite-range parameter of $1/\beta = 0.770$. The effects of nonlocality were corrected for by using the local-energy approximation of Perey and Saxon[38] with nonlocal ranges of $\beta_{^3\mathrm{He}} = 0.25$, $\beta_d = 0.54$, and $\beta_p = 0.85$. The quantity shown in Fig. 8 is the single-particle stripping cross section $\sigma_{nlj}(\theta)$, as calculated by code DWUCK. The calculations which include FRNL corrections are from 50 to 60% greater than the zero-range, local (ZRL) predictions; however, little difference is observed in the shapes from the two calculations. All theoretical calculations shown in Figs. 3–6 were made using the ZRL approximation and a lower radial-integral cutoff radius of zero. Spectroscopic factors were calculated for both FRNL and ZRL predictions.

Extracted spectroscopic factors were compared

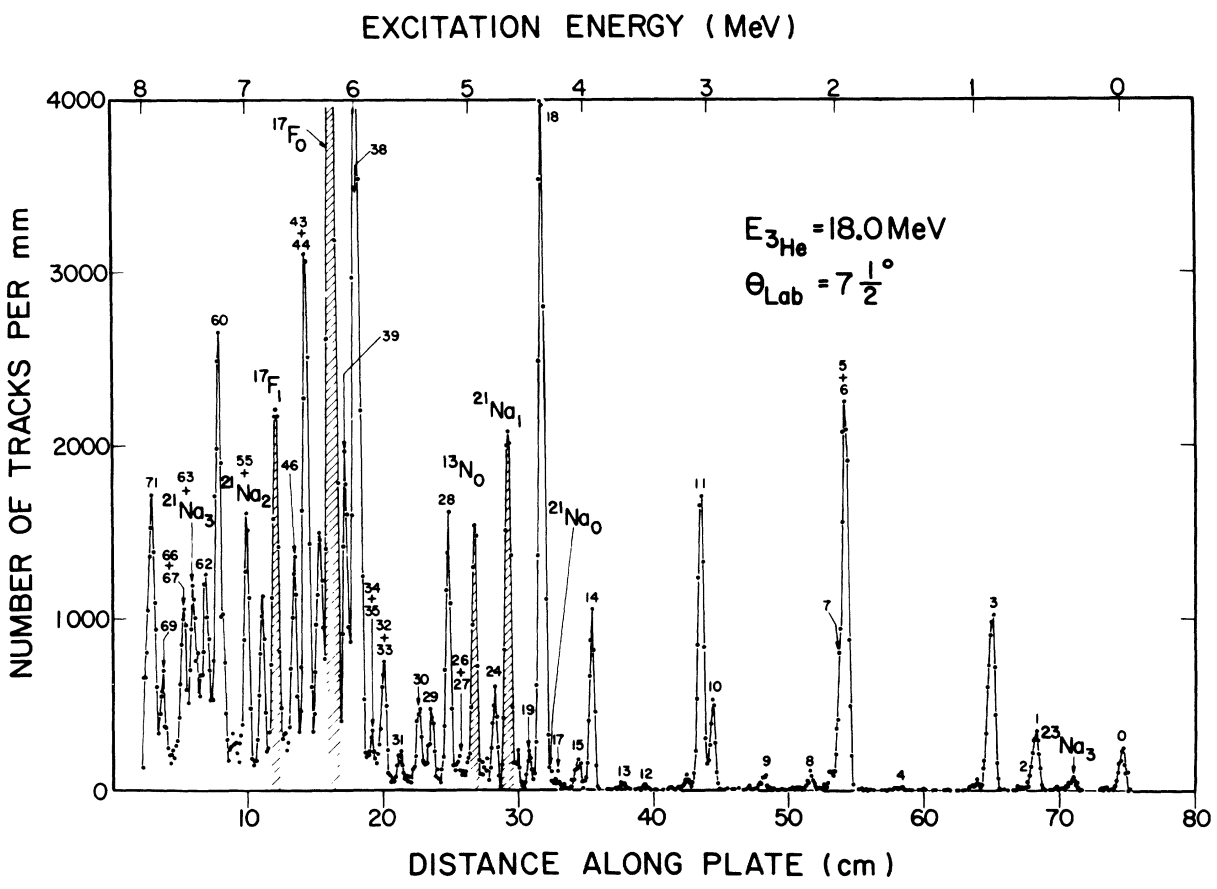

FIG. 2. Deuteron-momentum spectrum from the reaction ^{21}Ne(^{3}He, d)^{22}Na. Reaction products from target impurities are identified by the levels of the corresponding residual nucleus. The peak enumeration follows the level numbering of Table V and Ref. 1.

with those calculated using Satchler's formula[39]

$$C^2S_{nlj} = g^2 \frac{2J_i+1}{2J_f+1} |\langle f|i\rangle|^2 |\langle j(K_f \mp K_i) J_i \pm K_i | J_f K_f\rangle|^2 \times |\langle \chi_f | a^\dagger | \chi_i\rangle|^2 , \quad (3)$$

where C, S_{nlj}, J_i, J_f, and j are as defined above, and K_i and K_f are the initial and final projections of J on the nuclear-symmetry axis. $\langle f|i\rangle$ is the core overlap and is near unity for small changes in deformations between the initial and final states.

The quantity g is given by

$$g^2 = [1+\delta(K_i,0)][1+\delta(K_f,0)] . \quad (4)$$

The $|\chi\rangle$'s describe the motion of the extra-core nucleons in the deformed body-fixed system, and $a^\dagger(\nu)$ creates a nucleon with quantum numbers $\nu = nljmt_z$.

Assuming only two nucleons outside the core (strong-coupling limit), the properly antisymmetrized intrinsic wave function for an odd-odd nucleus is given by

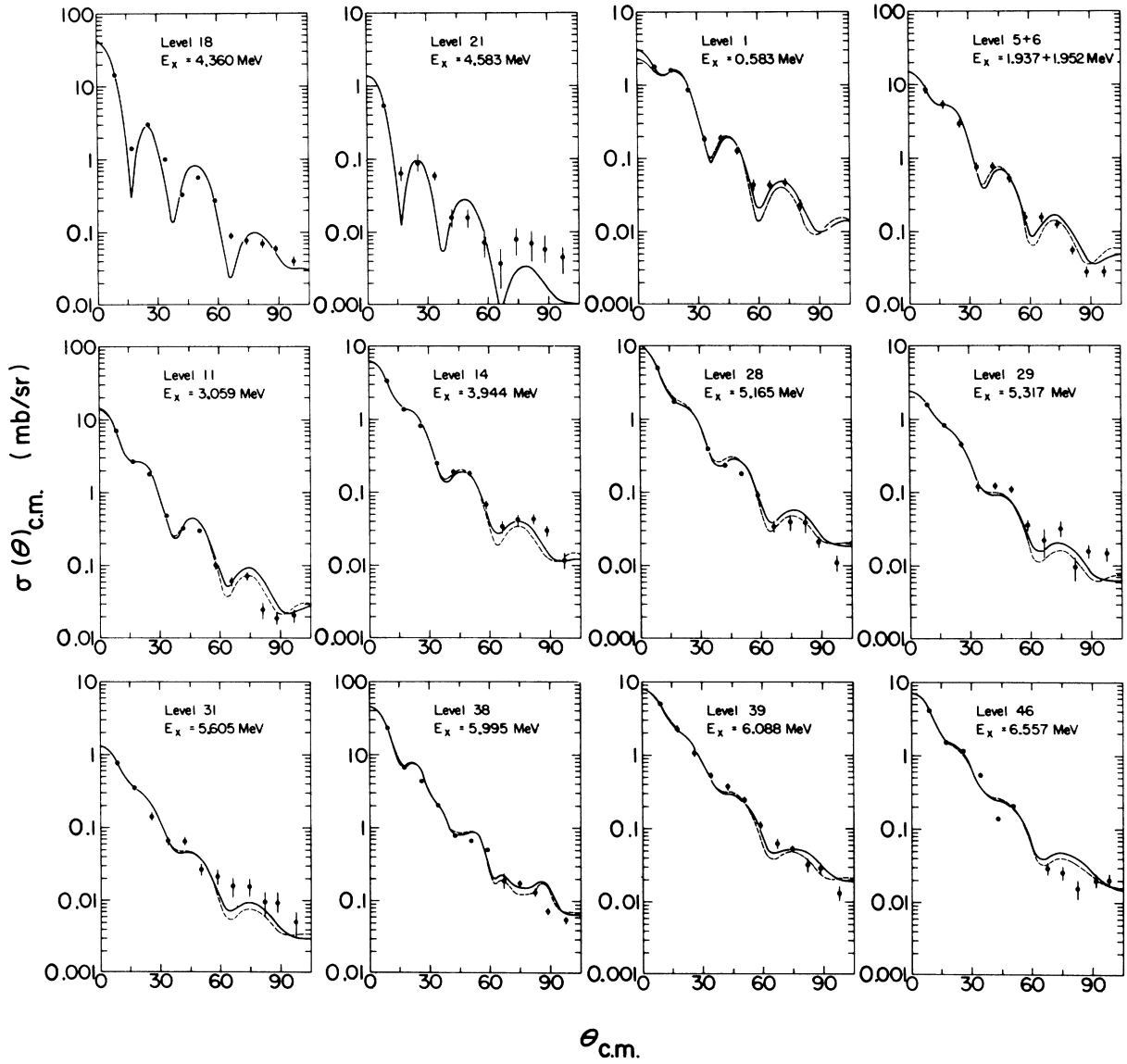

FIG. 3. Angular distributions exhibiting pure $l=0$ and $l=0+2$ admixed character in the ^{21}Ne(^{3}He,d)^{22}Na reaction. The DWBA curves shown with levels 18 and 21 were calculated for pure $l=0$ transitions. The remaining levels are shown with admixed $l=0$ and 2 predictions. The solid and dashed curves correspond, respectively, to $1d_{5/2}$ and $1d_{3/2}$ $l=2$ components.

$$|\chi_K\rangle = \frac{\chi_{\Omega_1}(n)\chi_{\Omega_2}(p) + (-1)^T \chi_{\Omega_1}(p)\chi_{\Omega_2}(n)}{\{2[1+\delta(\Omega_1,\Omega_2)]\}^{1/2}}, \quad (5)$$

where χ_Ω describes single-nucleon motion in a deformed potential well having spin projection Ω on the intrinsic z axis. Values of the matrix element of Eq. (3) are given in Table III for Nilsson states of ^{22}Na that may be populated by the ^{21}Ne-(^{3}He, d) reaction. For these calculations the ground state of ^{21}Ne, $|\chi_i\rangle$, is assumed to be a single unpaired neutron in the $\frac{3}{2}^+$ [211] Nilsson level outside a ^{20}Ne closed core. The $W(\alpha, \nu)$'s ($\alpha = N, n_z, \Lambda$, the Nilsson asymptotic quantum numbers[13]) are normalized expansion coefficients of the Nilsson wave functions in terms of a shell-model basis. Using the orthonormality of the Clebsch-Gordan coefficients and the normalization of the $W(\alpha, \nu)$'s, the in-band sum rules given in column five of Table III are obtained. The sum is over n, l, and j for all final states in a rotational band.

The Nilsson wave functions used in the calculation of spectroscopic factors were calculated[1,40] for a proton in a deformed Woods-Saxon well of mass 22. A deformed Thomas spin-orbit term of strength $\lambda = 25$ was included. Geometrical param-

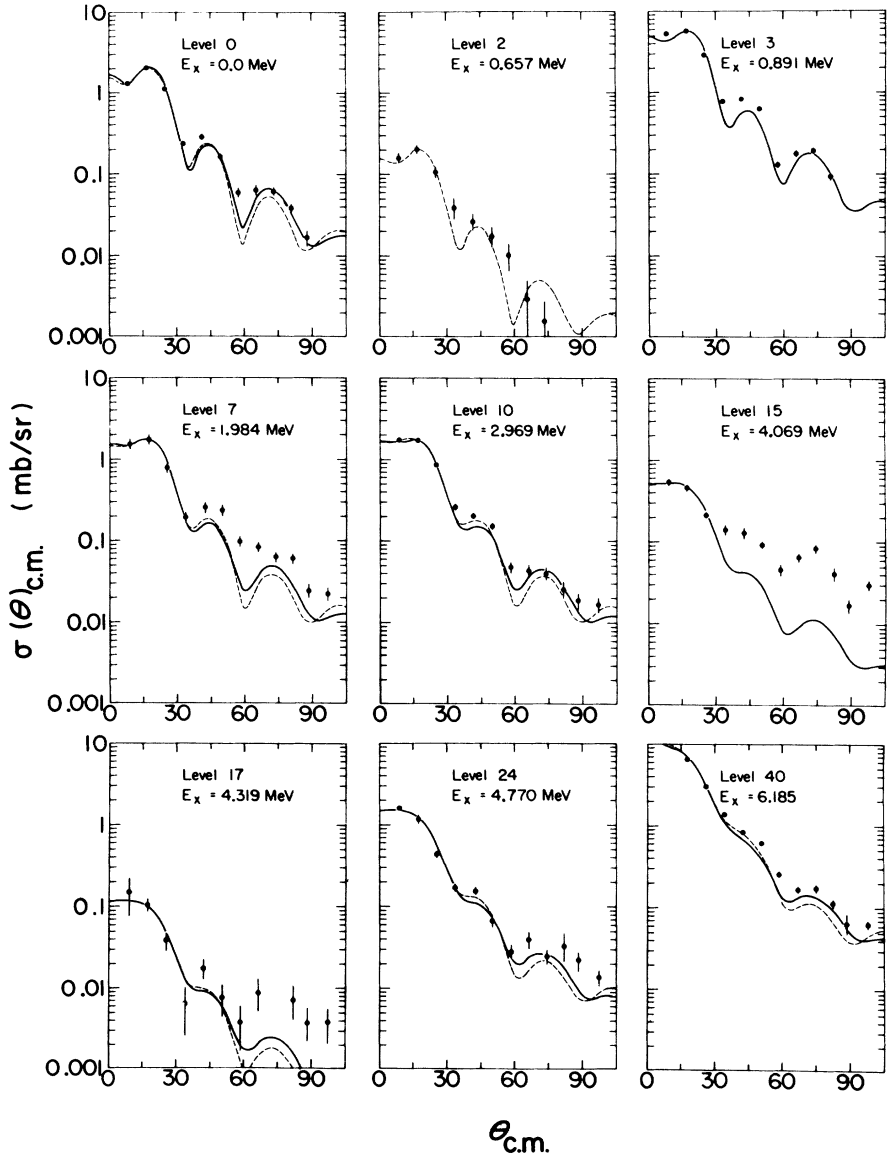

FIG. 4. Angular distributions exhibiting pure $l = 2$ character in the ^{21}Ne(^{3}He, d)^{22}Na reaction. The solid DWBA curves correspond to transfer to the $1d_{5/2}$ subshell and the dashed curves to the $1d_{3/2}$ subshell.

TABLE II. Optical-model parameters used in the DWBA calculations.

$$U(r)=V_C(r,\ r_C)-V_0\frac{1}{1+e^x}-iW\frac{1}{1+e^{x'}}+\left(\frac{\hbar}{M_\pi c}\right)^2 V_{so}\frac{1}{r}\frac{d}{dr}\left(\frac{1}{1+e^{x''}}\right)\vec{l}\cdot\vec{\sigma}$$

$$x=\frac{r-r_0A^{1/3}}{a},\quad x'=\frac{r-r_0'A^{1/3}}{a'},\quad x''=\frac{r-r_{so}A^{1/3}}{a_{so}}.$$

Channel	V_0 (MeV)	W (MeV)	W' (MeV)	$r_0=r_{so}$ (F)	$a=a_{so}$ (F)	r_C (F)	r_0' (F)	a' (F)	V_{so} (MeV)	Reference
^{21}Ne+^{3}He	177.0	13.0	···	1.138	0.7236	1.40	1.602	0.769	8.0	10[b]
^{22}Na+d	105.0	···	80.0	1.02	0.86	1.30	1.42	0.65	6.0	10[b,c]
Bound state	a	···	···	1.26	0.60	1.26	···	···	···	d

[a] The bound-state well depths were adjusted to give the nucleons a binding energy of $B=[5.494+Q(^3\text{He}, d)]$ MeV.
[b] H. T. Fortune, N. G. Puttaswamy, and J. L. Yntema, Phys. Rev. 185, 1546 (1969).
[c] J. L. Yntema and G. R. Satchler, Phys. Rev. 134, B976 (1964).
[d] H. T. Fortune, T. J. Gray, W. Trost, and N. R. Fletcher, Phys. Rev. 179, 1033 (1969).

eters of $V_0=51$ MeV, $r_0=1.25$ F, and $a=0.65$ F were used. Mixing among the first 13 major shells was included in the calculation. The resulting wave functions are given in Table IV in terms of a shell-model basis. Also shown for comparison are deformed harmonic-oscillator wave functions[41] for a deformation of $\delta=0.3$. Only amplitudes corresponding to orbits lower than 5 MeV unbound were calculated for the Woods-Saxon potential. Hence $\sum_{nlj}W(\alpha,\nu)^2$ (last column Table IV) is less than one. The predicted binding energies of the Woods-Saxon potential[1,40] are shown as a function of deformation in Fig. 9. The harmonic-oscillator results[41] are shown for comparison.

IV. RESULTS

The ^{21}Ne(^{3}He, d)^{22}Na angular distributions fall into six categories: (1) predominant $l=0$ (transitions to the 4.360- and 4.583-MeV levels); (2) $l=0$ and $l=2$ admixed (Fig. 3 other than the 4.360-

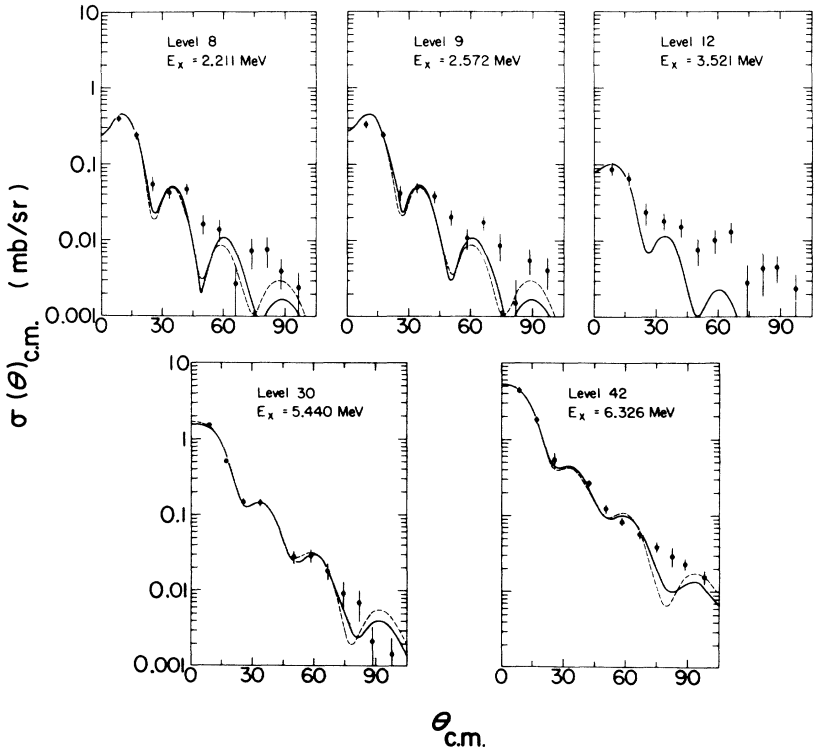

FIG. 5. Angular distributions exhibiting $l=1$ character in the ^{21}Ne(^{3}He, d)^{22}Na reaction. The solid DWBA curves correspond to transfer to the $2p_{3/2}$ subshell and the dashed curves to the $2p_{1/2}$ subshell.

TABLE III. Matrix elements and sum rules for predicting spectroscopic factors for various configurations [see Eq. (3) and text].

Configuration	K, T	$\lvert\langle\chi_f\lvert a^+\rvert\chi_i\rangle\rvert^2$	g^2	$\sum_{njl}^{I_f}\frac{2J_f+1}{2J_i+1}S_{nlj}$ [a]
$(\frac{3}{2}^+[211])^2$	0, 1	$\frac{1}{2}W(\alpha,\nu)^2$	2	$\sum_{njl} W(\alpha,\nu)^2$
$(\frac{3}{2}^+[211])^2$	0, 0	$\frac{1}{2}W(\alpha,\nu)^2$	2	$\sum_{njl} W(\alpha,\nu)^2$
$(\frac{3}{2}^+[211])^2$	3, 0	$W(\alpha,\nu)^2$	1	$2\sum_{njl} W(\alpha,\nu)^2$
b	c	$\frac{1}{2}W(\alpha,\nu)^2$	$1+\delta(K_f, 0)$	$\sum_{njl} W(\alpha,\nu)^2$

[a] For deformed harmonic-oscillator wave functions (Ref. 41) $\sum_{njl} W(\alpha,\nu)^2=1$; for wave functions calculated using Woods-Saxon potential see Table IV and text.

[b] Configurations where extra-core nucleons are not in same Nilsson orbit.

[c] $K=\Omega_1+\Omega_2$ or $\lvert\Omega_1-\Omega_2\rvert$. $T=0$ or 1.

and 4.583-MeV transitions); (3) predominant $l=2$ (Fig. 4); (4) $l=1$ (Fig. 5); (5) distributions which show considerable structure but do not fit into categories 1–4 (Fig. 6); and (6) weak cross sections showing little structure (Fig. 7).

In Fig. 3 the 4.360- and 4.583-MeV transitions are compared with $l=0$ DWBA predictions. The agreement for both states is good. Since the $l=0$ DWBA single-particle cross section at the angle of the forwardmost data point is approximately 10 times greater than that for $l=2$, a significant $l=2$ admixture could remain undetected. The cross section for the transition to the state at 4.583 MeV is very weak in comparison with an $l=0$ single-particle transition. A state at this excitation energy is observed to be populated by a strong $l=1$

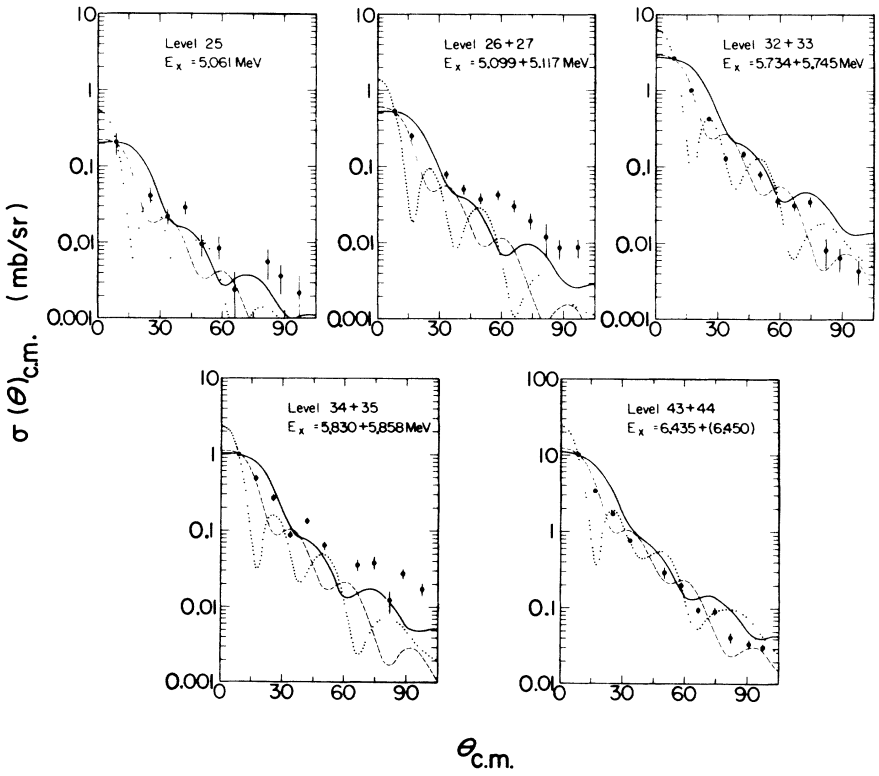

FIG. 6. Angular distributions which exhibit stripping-like structure that are not characteristic of $l=0$, 1, 2, or 0+2 transitions. The dotted, dashed, and solid DWBA curves correspond to $l=0$, 1, and 2 transitions, respectively.

^{23}Na(^{3}He, α) transition,[42] which is inconsistent with the $l=0$ (^{3}He, d) transition unless the two reactions populate different states.

The distributions of the remaining transitions in Fig. 3 are shown with admixed $l=0$ and $l=2$ predictions. The solid and broken curves are based on $1d_{5/2}$ and $1d_{3/2}$ final state $l=2$ configurations, respectively. The $l=0$ and $l=2$ admixtures were determined using a χ^2-minimization computer code. Again the stronger $l=0$ peak cross section may cause large errors in the magnitude of the $l=2$ admixture. The distinction between pure $l=2$ transitions and admixed $l=0$ and 2 transitions depends quite strongly on the magnitude of the most forward experimental point. This is especially true for transitions to the highest excited states where the forward minimum of the $l=2$ transition disappears (Fig. 4). Thus, spin assignments based on an $l=0$ component in the transitions to states at 0.583, 5.317, and 6.088 MeV must be considered as tentative. The stated "$l=1$ (^{3}He, d) transitions to the levels at 4.36 and 5.99 MeV" in the work of Garrett, Fortune, and Middleton[43] is in error. These levels are populated, respectively, by $l=0$ and admixed $l=0+2$ transitions (Fig. 3).

Angular distributions characteristic of $l=2$ and $l=1$ are presented in Figs. 4 and 5, respectively.

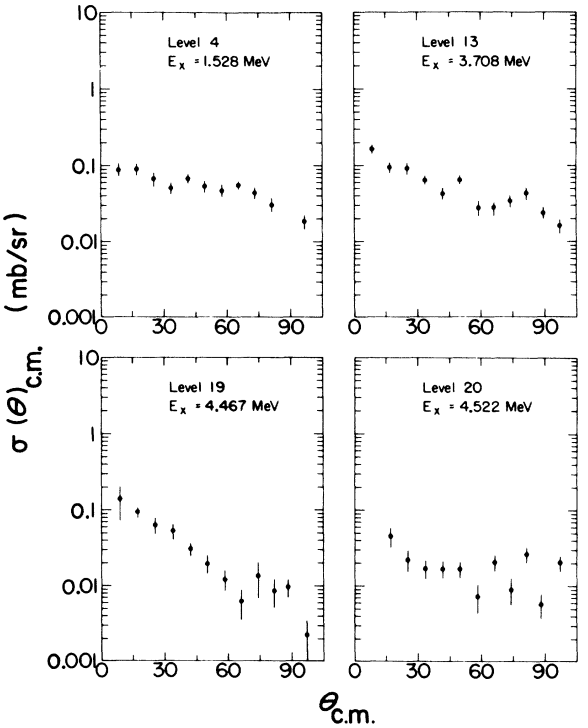

FIG. 7. Angular distributions for states excited weakly in the ^{21}Ne(^{3}He, d)^{22}Na reaction that are not characteristic of stripping.

In Fig. 4 the solid lines correspond to DWBA predictions based on $1d_{5/2}$ final-state configurations and the broken lines are $1d_{3/2}$ configurations. Similarly, in Fig. 5 the solid and broken lines are for $2p_{3/2}$ and $2p_{1/2}$ configurations. The most forward point of the 6.185-MeV (Fig. 4) transition was covered by reaction products due to a target impurity; thus a sizable $l=0$ admixture cannot be ruled out. The $l=1$ fit to the angular distribution of the weak transition to the 3.521-MeV level must be considered tentative. This distribution is included with the $l=1$ transitions because of the known $J^\pi=3^-$ assignment to this level.[16]

Figure 6 shows angular distributions of levels that exhibit considerable structure, but do not

TABLE IV. Eigenstates of the Nilsson Hamiltonian, calculated for a proton in a deformed Woods-Saxon well (see text for details of the calculation).

$\Omega^\pi[Nn_z\Lambda]$	δ [a]	$W(\alpha,\nu)$ $1p_{1/2}$	$1p_{3/2}$		$\sum_{ij} W^2$ [b]
$\frac{3}{2}^-[101]$	0.00		1.000		1.000
	0.30		1.000		1.000
	0.26		1.000		1.000
	0.53		0.996		0.992
$\frac{1}{2}^-[101]$	0.00	1.000	0.000		1.000
	0.30	0.912	0.411		1.000
	0.26	0.924	0.379		0.997
	0.53	0.864	0.487		0.984
		$2s_{1/2}$	$1d_{3/2}$	$1d_{5/2}$	
$\frac{5}{2}^+[202]$	0.00			1.000	1.000
	0.30			1.000	1.000
	0.26			0.998	0.996
	0.53			0.983	0.966
$\frac{3}{2}^+[211]$	0.00		0.000	1.000	1.000
	0.30		−0.252	0.968	1.000
	0.26		−0.241	0.975	0.997
	0.53		−0.335	0.939	0.992
$\frac{1}{2}^+[220]$	0.00	0.000	0.000	1.000	1.000
	0.30	−0.533	−0.306	0.789	1.000
	0.26	−0.441	−0.223	0.864	0.991
	0.53	−0.526	−0.383	0.742	0.974
$\frac{1}{2}^+[211]$	0.00	1.000	0.000	0.000	1.000
	0.30	0.370	0.754	0.543	1.000
	0.26	0.664	0.562	0.488	0.994
	0.53	0.260	0.758	0.584	0.982
$\frac{1}{2}^+[200]$	0.00	0.000	1.000	0.000	1.000
	0.30	−0.761	0.581	−0.288	1.000
	0.26	−0.598	0.790	−0.094	0.991
	0.53	−0.740	0.401	−0.259	0.775

[a] Tabulated values for $\delta=0.30$ are for oscillator potential (Ref. 41). Tabulated values for $\delta=0.26$ and 0.52 are for Woods-Saxon well (Refs. 1 and 37).

[b] The Woods-Saxon well calculations include mixing among the first 13 major shells. Consequently, $\sum_{ij} W^2$ is less than 1.0 for a sum over l and j of only one shell.

fit nicely into one of the categories discussed above (i.e., $l=0$, 1, 2, or 0+2 admixed). Except for the weak 5.061-MeV transition, these distributions are sums of known unresolved transitions. The solid DWBA curves were calculated for $l=2$ proton transfer, the dashed curves for $l=1$ transfer, and the dotted curves for $l=0$ transfer. The 5.099+5.117-MeV transition seems to resemble the $l=1$ DWBA curve most closely.

The angular distributions shown in Fig. 7 are for weaker transitions that do not exhibit stripping-like structure. The state at 1.528 MeV is known to have $J^\pi=5^+$ and that at 3.708 MeV is thought to have $J^\pi=6^+$.[16] Consequently, these states could not be populated directly by adding a single nucleon to the s-d shell.

Spectroscopic factors extracted using Eq. (1) are given in Table V for the states whose angular distributions were compared with DWBA predictions. The normalization constant, N, for the ZRL-DWBA calculations was taken to be 4.42.[44] The isospin coupling coefficient C^2 equals $\frac{1}{2}$ for ^{21}Ne-(^{3}He, d) transitions to both $T=0$ and $T=1$ final states in ^{22}Na. If $l=1$ calculated single-particle cross sections were based on adding a proton to the $1p$ shell instead of the $2p$ shell, the tabulated $l=1$ spectroscopic factors would be increased by from a factor of 2 (for $E_x=6.33$ MeV) to 2.5 (for $E_x=2.21$ MeV).

The absolute spectroscopic factor depends directly on the absolute cross-section measurement and the absolute magnitude of the DWBA predictions. Since significant uncertainties exist in both of these quantities (e.g., a 20% uncertainty has already been placed on the absolute cross section and the uncertainty in the DW analysis is probably even greater), a test of the absolute normalization for this particular study is desired. The rotational-band sum rule (given in Table III) provides such a test using the ground-state $K=3$ band based on the $(\frac{3}{2}^+[211])^2$ Nilsson configuration The low-lying members of this band (ground state, $J^\pi=3^+$; 0.891 MeV, $J^\pi=4^+$; and 1.528 MeV, $J^\pi=5^+$) are well established (see Table I). Assuming the Nilsson model, the 3^+ member of this band is predicted to be excited predominantly by the transfer of a $1d_{5/2}$ proton (see Table VIII). The 4^+ state can be excited only by $1d_{5/2}$ transfer, and the higher members cannot be excited directly. Renormalization using this model-dependent method yields empirical normalization constants of 5.97 for the ZRL calculations and 3.70 for FRNL. The renormalized spectroscopic factors are given in columns 8 and 9 of Table V for ZRL- and FRNL-DWBA calculations, respectively. These renormalized spectroscopic factors are about 25% less than those calculated using the normally accepted value of 4.42 for the ZRL normalization constant. This agreement lends support to our absolute cross sections and the DWBA calculations. An excepted uncertainty of 35% is assigned to the measured spectroscopic factor when only one l contributes to the transition. When the transition proceeds by two l values, a 50% uncertainty is assigned because of errors induced in the empirical separation. Spectroscopic factors calculated assuming $N=4.42$ will be used (except where otherwise stated) in the following discussion and conclusions.

Table VI presents upper limits on spectroscopic

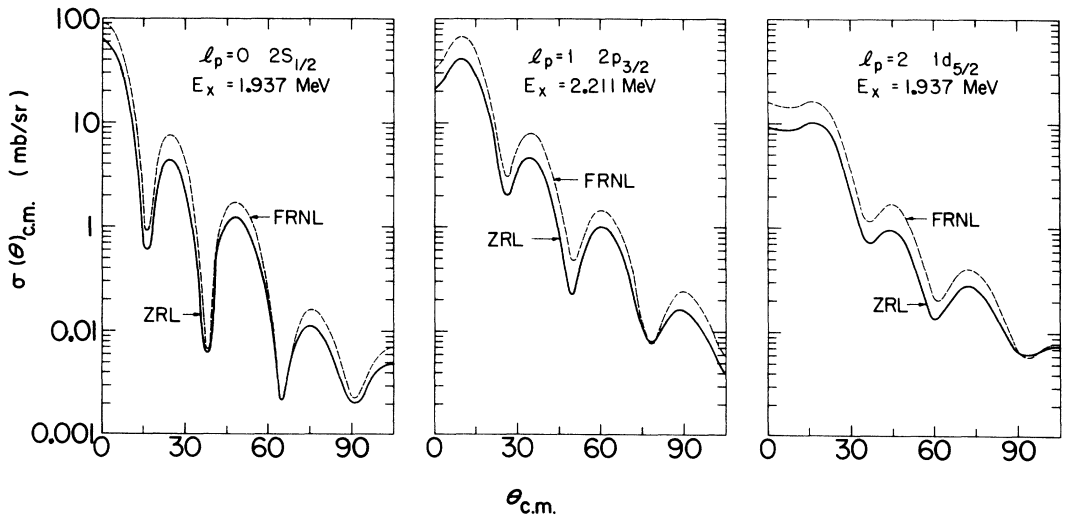

FIG. 8. Comparison of zero-range local (ZRL)- and finite-range nonlocal (FRNL)-DWBA predictions for the ^{21}Ne(^{3}He, d)^{22}Na reaction. See Table II and the text for the parameters used in the calculations.

TABLE V. Results of the ^{21}Ne(^{3}He, d)^{22}Na reaction.

Level No.	E_x [a] (MeV)	J^π lit [b]	l_p [c]	Assignment [c]	j_p	$(2J_f+1)C^2S$ ZRL [d]	ZRL [e]	FRNL [f]
0	0.0	3^+	2		$\frac{5}{2}$	1.66	1.23	1.18
					$\frac{3}{2}$	2.33	1.72	1.70
1	0.583	1^+	(0) + 2		$\frac{5}{2}$	0.977	0.723	0.662
					$\frac{1}{2}$	0.058	0.043	0.030
					$\frac{3}{2}$	1.60	1.18	1.09
					$\frac{1}{2}$	0.033	0.024	0.024
2	0.657	0^+; 1	2		$\frac{3}{2}$	<0.203	<0.150	<0.149
3	0.891	4^+	2		$\frac{5}{2}$	3.75	2.77	2.82
4	1.528	5^+	g					
5	1.937	1^+	0 + 2		$\frac{5}{2}$	2.50	1.85	1.96
6	1.952	2^+; 1			$\frac{1}{2}$	0.293	0.217	0.208
					$\frac{3}{2}$	3.80	2.81	2.88
					$\frac{1}{2}$	0.282	0.209	0.197
7	1.984	3^+	2		$\frac{5}{2}$	0.934	0.692	0.694
					$\frac{3}{2}$	1.34	0.992	0.943
8	2.211	1^-	1		$\frac{3}{2}$	0.040	0.030	0.028
					$\frac{1}{2}$	0.045	0.033	0.031
9	2.572	2^-	1		$\frac{3}{2}$	0.042	0.031	0.028
					$\frac{1}{2}$	0.047	0.035	0.035
10	2.969	3^+	2		$\frac{5}{2}$	0.793	0.587	0.584
					$\frac{3}{2}$	1.12	0.829	0.804
11	3.059	2^+	0 + 2		$\frac{5}{2}$	0.956	0.708	0.739
					$\frac{1}{2}$	0.306	0.227	0.227
					$\frac{3}{2}$	1.40	1.04	1.04
					$\frac{1}{2}$	0.300	0.222	0.223
12	3.521	3^-	(1)		$\frac{3}{2}$	<0.009	<0.007	<0.007
13	3.708	(6^+)	g					
14	3.944	1^+	0 + 2		$\frac{5}{2}$	0.495	0.366	0.370
					$\frac{1}{2}$	0.152	0.113	0.117
					$\frac{3}{2}$	0.680	0.503	0.454
					$\frac{1}{2}$	0.153	0.113	0.112
15	4.069	$(4^+, 1)$	2	$\pi = +$	$\frac{5}{2}$	0.185	0.137	0.136
16	4.294		h					
17	4.319	1^+	(2)		$\frac{5}{2}$	0.038	0.028	0.028
					$\frac{3}{2}$	0.051	0.038	0.040
18	4.360	2(1)	0	$\pi = +$	$\frac{1}{2}$	1.66	1.23	1.34
19	4.466		g					
20	4.522		g					
21	4.583		(0) [i]		$\frac{1}{2}$	0.060	0.044	0.047

TABLE V *(Continued)*

Level No.	E_x [a] (MeV)	J^π lit [b]	l_p [c]	Assignment [c]	j_p	$(2J_f+1)C^2S$ ZRL [d]	ZRL [e]	FRNL [f]
22	4.622	1	j					
23	4.708	(3^+, 4^+, 5^+)	h					
24	4.770		2	0^+, 1^+, 2^+, 3^+, 4^+	$\frac{5}{2}$	0.467	0.346	0.354
					$\frac{3}{2}$	0.615	0.455	0.476
25	5.061	≥1	k					
26	5.099		k					
27	5.117							
28	5.165	(2^+, 1)	0+2	$\pi=+$	$\frac{5}{2}$	0.494	0.366	0.383
					$\frac{1}{2}$	0.319	0.236	0.259
					$\frac{3}{2}$	0.695	0.515	0.523
					$\frac{1}{2}$	0.309	0.229	0.251
29	5.317		(0)+2	1^+, 2^+ (0^+, 3^+, 4^+)	$\frac{5}{2}$	0.260	0.192	0.208
					$\frac{1}{2}$	0.065	0.048	0.050
					$\frac{3}{2}$	0.356	0.264	0.277
					$\frac{1}{2}$	0.062	0.046	0.045
30	5.440		1	0^-, 1^-, 2^-, 3^-	$\frac{3}{2}$	0.134	0.099	0.104
					$\frac{1}{2}$	0.154	0.113	0.117
31	5.605		0+2	1^+, 2^+	$\frac{5}{2}$	0.104	0.077	0.085
					$\frac{1}{2}$	0.044	0.033	0.035
					$\frac{3}{2}$	0.140	0.104	0.108
					$\frac{1}{2}$	0.043	0.032	0.032
32	5.734*	One level	k					
33	5.745*	0^+, 1^+						
34	5.830		k					
35	5.858							
36	5.938*		m					
37	5.953*		m					
38	5.995 [n]		0+2	1^+, 2^+	$\frac{5}{2}$	1.99	1.47	1.52
					$\frac{1}{2}$	1.41	1.04	1.18
					$\frac{3}{2}$	2.45	1.81	1.98
					$\frac{1}{2}$	1.44	1.07	1.16
39	6.088		(0)+2	1^+, 2^+(0^+, 3^+, 4^+)	$\frac{5}{2}$	0.695	0.515	0.564
					$\frac{1}{2}$	0.362	0.268	0.281
					$\frac{3}{2}$	0.963	0.713	0.761
					$\frac{1}{2}$	0.335	0.248	0.253
40	6.185 [n]		2	0^+, 1^+, 2^+, 3^+, 4^+	$\frac{5}{2}$	3.09	2.29	1.95
					$\frac{3}{2}$	3.51	2.60	2.68

TABLE V *(Continued)*

Level No.	E_x [a] (MeV)	J^π lit [b]	l_p [c]	Assignment [c]	j_p	$(2J_f+1)C^2S$ ZRL [d]	ZRL [e]	FRNL [f]
41	6.247		j					
42	6.326		1	1^-, 2^-, $(0^-, 3^-)$	$\frac{3}{2}$	0.525	0.389	0.406
					$\frac{1}{2}$	0.561	0.415	0.432
43	6.435*		k					
44	6.450*							
45	6.521		m					
46	6.557		0+2	1^+, 2^+	$\frac{5}{2}$	0.528	0.391	0.357
					$\frac{1}{2}$	0.455	0.337	0.396
					$\frac{3}{2}$	0.623	0.461	0.467
					$\frac{1}{2}$	0.449	0.332	0.381

[a] Energies from Ref. 16 for levels below 5.4 MeV, and from Ref. 1 for those above 5.4 except for energies marked by an asterisk where they are from Ref. 17.
[b] See Ref. 1.
[c] Parentheses indicate tentative assignment.
[d] Based on normally accepted (Ref. 41) $N=4.42$.
[e] Based on empirical renormalization using ground-state band (see text).
[f] Based on empirical renormalization using ground-state band (see text).
[g] No stripping pattern observed.
[h] State not excited.
[i] See text.
[j] State covered by impurity.
[k] See Fig. 6 and Table VI.
[m] Covered by neighboring strongly excited states.
[n] Possible doublet – see text.

factors for the levels whose angular distributions are presented in Fig. 6. These distributions are not characteristic of $l=0$, 1, 2, or 0+2 admixed.

Information regarding the filling of the ^{22}Na configurations may be obtained using the appropriate single-nucleon-transfer sum rule[45]:

$$\sum \frac{2I_f+1}{2I_i+1} C^2S_{lj} = N_{lj}. \tag{6}$$

The sum extends over all states with the same l and j. N_{lj} is the number of proton holes in the lj orbital. The summed $l=0$, 1, and 2 ^{21}Ne(^{3}He, d) spectroscopic strengths up to 6.6 MeV are presented in Table VII. [The spectroscopic factors for the levels that are not characteristic of a particular l transfer (see Fig. 6 and Table VI) are not included in the sums.] Assuming that the ground-state configuration of ^{21}Ne has four $1d_{5/2}$ proton holes and all higher configuraations are empty, $N_{lj}=4$, 2, and 4, respectively, for the $1d_{5/2}$, $2s_{1/2}$, and $1d_{3/2}$ orbitals. It is obvious that considerable $2s$-$1d$ shell-stripping strength is not accounted for below 6.6 MeV.

Spectroscopic factors, calculated using Eq. (3) and the Woods-Saxon potential wave functions (Table IV), are presented in Table VIII. For calculations based on the $\frac{1}{2}^-[330]$ orbit, wave functions for a neutron[1] (rather than a proton) in a Woods-Saxon well were used. The geometry of the well for the neutrons was the same as that of the protons described in Sec. III. The proton and neutron wave functions for otherwise identical quantum numbers differ by no more than 10% in amplitude for any component. The predicted spectroscopic factors are based on adding a proton to the ^{21}Ne ground state, assumed to be an unpaired neutron in the $\frac{3}{2}^+[211]$ Nilsson orbit will all lower orbits filled (Fig. 9). Whenever a specific final state of ^{22}Na is associated with a rotational-band member, its excitation energy is listed in column 4 and its measured spectroscopic factor is listed in column 5. When it is possible for the transfer to proceed by two j's (e.g., $j=\frac{3}{2}$ and $\frac{5}{2}$ for $l=2$), the tabulated experimental spectroscopic factor, S_{exp}, is for the j corresponding to the larger predicted spectroscopic factor S_{th}. When two j's contribute, the sum of the two predicted spectroscopic factors, S_{th}, should be compared with S_{exp}. The experimental spectroscopic factors included in Table VIII are all based on ZRL calculations

and a normalization constant of 4.42. If the empirical normalization based on the sum rule for the ground-state band were used, the experimental spectroscopic factors would be reduced by about 25%.

V. DISCUSSION

A. States Based on the $(\frac{3}{2}^+[211])^2$ Nilsson Configuration

Three rotational bands based on placing an extra-core neutron and proton in the $\frac{3}{2}^+[211]$ Nilsson orbital have previously been suggested[1,2,16] (see Table I). Figure 10 compares predicted and measured ^{21}Ne(^{3}He, d) $l=2$ spectroscopic factors for the levels in these bands that may be populated by single-nucleon stripping. (The transition to the $J^\pi = 2^+$, $T=1$ level at 1.952 MeV is not included since the deuterons for this transition are not resolved from those corresponding to the level at 1.937 MeV.) The solid horizontal lines are the experimental spectroscopic factors, and the hashed area corresponds to the assigned errors. (See Sec. IV.) When it is possible for the transfer to proceed by two j's, the spectroscopic factor shown corresponds to the j value having the larger predicted spectroscopic factor. The curves in Fig. 10 are the predicted spectroscopic factor as a function of the deformation. With the exception of the transition to the level at 0.657 MeV, these predicted spectroscopic factors are not strong functions of deformation, and the agreement of

TABLE VI. Upper limit of ^{21}Ne(^{3}He, d)^{22}Na spectroscopic factors for transitions to levels shown in Fig. 6.

Level No.	E_x (MeV)	l_p	j_p	$(2J_f+1)C^2S$ [a]
25	5.061	2	$\frac{5}{2}$	0.061
			$\frac{3}{2}$	0.080
		1	$\frac{3}{2}$	0.020
			$\frac{1}{2}$	0.021
		0	$\frac{1}{2}$	0.026
26+27	5.099+5.117	2	$\frac{5}{2}$	0.152
			$\frac{3}{2}$	0.203
		1	$\frac{3}{2}$	0.052
			$\frac{1}{2}$	0.059
		0	$\frac{1}{2}$	0.071
32+33	5.734+5.745	2	$\frac{5}{2}$	0.739
			$\frac{3}{2}$	0.995
		1	$\frac{3}{2}$	0.253
			$\frac{1}{2}$	0.268
		0	$\frac{1}{2}$	0.376
34+35	5.830+5.858	2	$\frac{5}{2}$	0.283
			$\frac{3}{2}$	0.362
		1	$\frac{3}{2}$	0.098
			$\frac{1}{2}$	0.108
		0	$\frac{1}{2}$	0.147
43+44	6.435+6.450	2	$\frac{5}{2}$	2.61
			$\frac{3}{2}$	3.44
		1	$\frac{3}{2}$	1.28
			$\frac{1}{2}$	1.36
		0	$\frac{1}{2}$	2.71

[a] Based on ZRL calculations and $N=4.42$ (see text).

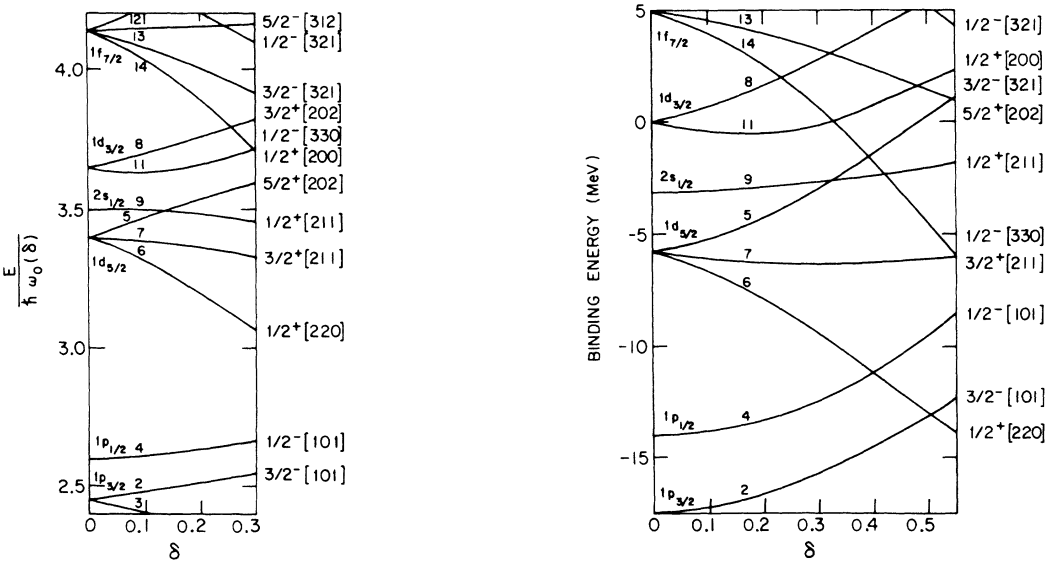

FIG. 9. Binding energies of proton states (right) as calculated in a deformed Woods-Saxon potential (see text). Also shown for comparison are the deformed harmonic-oscillator calculations of Chi (left; Ref. 41). The results are shown for positive deformations as a function of the Nilsson ellipsoidal-deformation parameter δ.

TABLE VII. Summed spectroscopic strengths.

l	Assumed j	$\sum_{I_f} \frac{2J_f+1}{2J_i+1} C^2S_{lj}$ ZRL[a]	ZRL[b]	FRNL[b]
2	$\frac{5}{2}$	5.02	3.71	3.67
	$\frac{3}{2}$	6.85	5.06	5.16
1	$\frac{3}{2}$	0.19	0.14	0.14
	$\frac{1}{2}$	0.20	0.15	0.16
0	$\frac{1}{2}$	1.30	0.96	1.04

[a] Based on normally accepted (Ref. 44) $N = 4.42$.
[b] Based on empirical renormalization using ground-state band (see text).

the predicted and measured spectroscopic factors is within the expected uncertainties for all deformations. For the transition to the 0.657-MeV level, satisfactory agreement is obtained only for deformations of $\delta \gtrsim 0.4$. This large deformation is consistent with previous works in this mass region.[1-5] The (^{3}He, d) transitions to states based on this configuration are predicted to proceed by pure $l = 2$ proton transfer, since the transferred proton enters an orbit having $\Omega^\pi = \frac{3}{2}^+$. A small $l = 0$ component ($S_{exp} = 0.04$) is probably observed (Fig. 3) in the transition to the $J^\pi = 1^+$ state at 0.583 MeV.

B. States Based on the $\frac{3}{2}^+[211]$, $\frac{1}{2}^+[211]$ Nilsson Configuration

The $(\frac{3}{2}^+[211])^2$ configuration can account for all the positive-parity levels below 2.9 MeV with the exception of the 1^+ level at 1.937 MeV. The next lowest single-particle configuration (Fig. 9) would be $\frac{3}{2}^+[211]$, $\frac{5}{2}^+[202]$ having $K = 1$ and 4 rotational bands or $\frac{3}{2}^+[211]$, $\frac{1}{2}^+[211]$ having $K = 1$ and 2 bands. States based on transferring a proton to the $\frac{5}{2}^+[202]$ orbit should be populated by pure $l = 2$ (^{3}He, d) transitions. A sizable $l = 0$ (^{3}He, d) transition [$(2J_f + 1)S_{exp} = 0.58$] is observed to the 1.937-1.952-MeV doublet. The transition to the 1.952-MeV member should be pure $l = 2$, assuming that this state is based on the $(\frac{3}{2}^+[211])^2$ Nilsson configuration. Because of the observed $l = 0$ transition and the belief that ^{22}Na possesses a large deformation (the $\frac{1}{2}^+[211]$ Nilsson level is predicted to lie lower than the $\frac{5}{2}^+[202]$ level for deformations greater than $\delta \approx 0.32$), the 1.937-MeV 1^+ level is tentatively identified as the $\frac{3}{2}^+[211]$, $\frac{1}{2}^+[211]$ $K = 1$ band head. The $\frac{3}{2}^+[211]$, $\frac{1}{2}^+[211]$ band heads are, however, predicted to lie above 4 MeV in excitation (see Fig. 9). If the 1.952-MeV state has no $l = 0$ strength, the predicted and measured $l = 0$ (^{3}He, d) spectroscopic factors for the 1.937-MeV level agree for deformations of $0.35 \leq \delta \leq 0.50$ (Fig. 11).

The 3.059-MeV 2^+ state is at the proper excita-

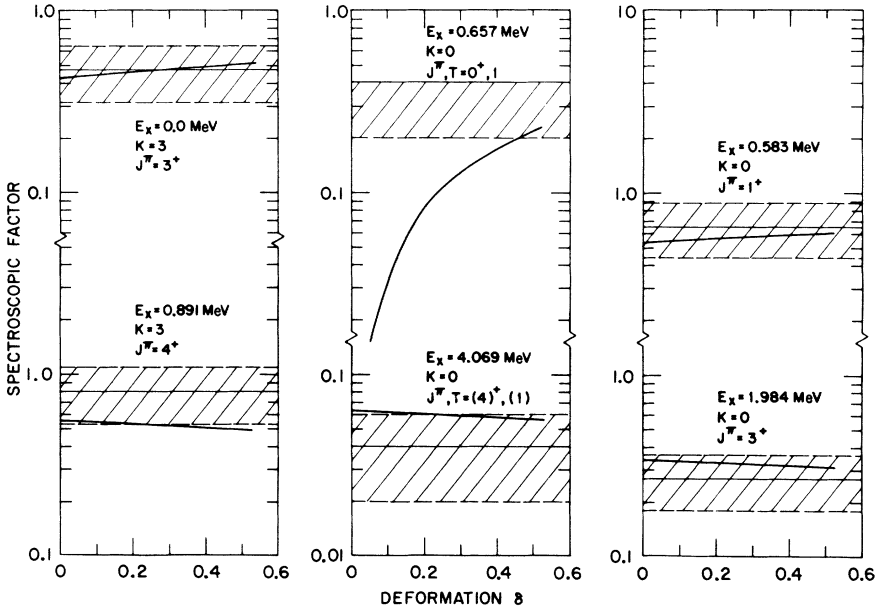

FIG. 10. Comparison of predicted and measured $l = 2$ spectroscopic factors for states based on the $(\frac{3}{2}^+[211])^2$ Nilsson configuration. The solid horizontal lines are the experimental values (based on the ZRL-DWBA calculations and $N = 4.42$) and the dashed area represents the assigned errors. When it is possible for the transfer to proceed by two j's, the experimental value shown corresponds to the j having the larger predicted spectroscopic factor. The curves are the predictions of the rotational model (see text) as a function of the deformation.

TABLE VIII. Comparison of measured and predicted ^{21}Ne(^{3}He, d)^{22}Na spectroscopic factors.

Configuration ($\Omega^\pi[Nn_z\Lambda]$)	K	J^π [a]	E_x [b] (MeV)	S_{exp} [c]	l	j	S_{th} [d] $\delta=0.0$	$\delta=0.2625$	$\delta=0.525$
$(\frac{3}{2}^+[211])^2$	3	3^+, $T=0$	0.0	0.47	2	$\frac{5}{2}$	0.43	0.41	0.38
						$\frac{3}{2}$	0.00	0.06	0.13
		4^+, $T=0$	0.891	0.80	2	$\frac{5}{2}$	0.56	0.53	0.49
$(\frac{3}{2}^+[211])^2$	0	0^+, $T=1$	0.657	<0.40	2	$\frac{3}{2}$	0.00	0.10	0.22
		2^+, $T=1$	1.952	d	2	$\frac{5}{2}$	0.69	0.65	0.60
						$\frac{3}{2}$	0.00	0.02	0.04
		4^+, $T=1$	4.069	0.04	2	$\frac{5}{2}$	0.06	0.06	0.06
$(\frac{3}{2}^+[211])^2$	0	1^+, $T=0$	0.583	0.65	2	$\frac{5}{2}$	0.53	0.51	0.47
						$\frac{3}{2}$	0.00	0.06	0.13
		3^+, $T=0$	1.984	0.27	2	$\frac{5}{2}$	0.34	0.33	0.30
						$\frac{3}{2}$	0.00	0.00	0.01
$\frac{3}{2}^+[211]$, $\frac{1}{2}^+[211]$	1	1^+	1.937	e	2	$\frac{5}{2}$	0.00	0.02	0.02
						$\frac{3}{2}$	0.00	0.13	0.23
				0.20	0	$\frac{1}{2}$	1.00	0.44	0.06
		2^+	(3.059)	0.56	2	$\frac{5}{2}$	0.00	0.06	0.09
						$\frac{3}{2}$	0.00	0.13	0.23
				0.12	0	$\frac{1}{2}$	0.20	0.09	0.01
		3^+	(4.770)	0.13	2	$\frac{5}{2}$	0.00	0.06	0.09
						$\frac{3}{2}$	0.00	0.04	0.07
		4^+			2	$\frac{5}{2}$	0.00	0.02	0.03
$\frac{3}{2}^+[211]$, $\frac{1}{2}^+[211]$	2	2^+	(5.165, $T=1$)	0.28	2	$\frac{5}{2}$	0.00	0.03	0.04
						$\frac{3}{2}$	0.00	0.13	0.23
				0.12	0	$\frac{1}{2}$	0.80	0.35	0.05
		3^+			2	$\frac{5}{2}$	0.00	0.07	0.10
						$\frac{3}{2}$	0.00	0.09	0.17
		4^+			2	$\frac{5}{2}$	0.00	0.04	0.05
$\frac{3}{2}^+[211]$, $\frac{5}{2}^+[202]$	1	1^+	(3.944)	0.33	2	$\frac{5}{2}$	0.67	0.67	0.67
		2^+			2	$\frac{5}{2}$	0.29	0.29	0.29
		3^+			2	$\frac{5}{2}$	0.07	0.07	0.07
		4^+			2	$\frac{5}{2}$	0.01	0.01	0.01
$\frac{3}{2}^+[211]$, $\frac{5}{2}^+[202]$	4	4^+			2	$\frac{5}{2}$	0.44	0.44	0.44
$\frac{3}{2}^+[211]$, $\frac{1}{2}^+[200]$	1	1^+	(4.360, 5.995)	<0.1, 1.63	2	$\frac{5}{2}$	0.00	0.00	0.01
						$\frac{3}{2}$	0.40	0.25	0.06
				1.10, 0.96	0	$\frac{1}{2}$	0.00	0.36	0.55
		2^+			2	$\frac{5}{2}$	0.00	0.00	0.02
					2	$\frac{3}{2}$	0.40	0.25	0.06
					0	$\frac{1}{2}$	0.00	0.07	0.11
		3^+			2	$\frac{5}{2}$	0.00	0.00	0.02
						$\frac{3}{2}$	0.11	0.07	0.02

TABLE VIII *(Continued)*

Configuration ($\Omega^\pi[Nn_z\Lambda]$)	K	J^π [a]	E_x [a] (MeV)	S_{exp} [c]	l	j	S_{th} [d] $\delta=0.0$	$\delta=0.2625$	$\delta=0.525$
		4^+			2	$\frac{5}{2}$	0.00	0.00	0.01
$\frac{3}{2}^+[211]$, $\frac{1}{2}^+[200]$	2	2^+	(4.360, 5.995)	<0.07, 0.98	2	$\frac{5}{2}$	0.00	0.00	0.01
						$\frac{3}{2}$	0.40	0.25	0.06
				0.66, 0.58	0	$\frac{1}{2}$	0.00	0.29	0.44
		3^+			2	$\frac{5}{2}$	0.00	0.00	0.02
						$\frac{3}{2}$	0.29	0.18	0.05
		4^+			2	$\frac{5}{2}$	0.00	0.00	0.01
$\frac{3}{2}^+[211]$, $\frac{1}{2}^-[330]$	1	1^-	(6.326)		3	$\frac{5}{2}$	0.00	<0.01	<0.02
				0.37	1	$\frac{3}{2}$	0.00	0.16	0.13
						$\frac{1}{2}$	0.00	0.05	0.09
		2^-			3	$\frac{7}{2}$	0.06	0.03	0.02
						$\frac{5}{2}$	0.00	<0.02	<0.06
					1	$\frac{3}{2}$	0.00	0.16	0.13
						$\frac{1}{2}$	0.00	0.01	0.02
		3^-			3	$\frac{7}{2}$	0.19	0.09	0.07
						$\frac{5}{2}$	0.00	<0.02	<0.06
					1	$\frac{3}{2}$	0.00	0.05	0.04
		4^-			3	$\frac{7}{2}$	0.19	0.09	0.07
						$\frac{5}{2}$	0.00	<0.01	<0.02
		5^-			3	$\frac{7}{2}$	0.06	0.03	0.02
$\frac{3}{2}^+[211]$, $\frac{1}{2}^-[330]$	2	2^-	(6.326)		3	$\frac{7}{2}$	0.01	0.01	0.01
						$\frac{5}{2}$	0.00	<0.01	<0.03
				0.22	1	$\frac{3}{2}$	0.00	0.16	0.13
						$\frac{1}{2}$	0.00	0.04	0.07
		3^-			3	$\frac{7}{2}$	0.12	0.06	0.04
						$\frac{5}{2}$	0.00	<0.02	<0.06
					1	$\frac{3}{2}$	0.00	0.12	0.10
		4^-			3	$\frac{7}{2}$	0.21	0.10	0.08
						$\frac{5}{2}$	0.00	<0.01	<0.03
		5^-			3	$\frac{7}{2}$	0.11	0.05	0.04

[a] Both $T=0$ and 1 components are allowed for configurations other than $(\frac{3}{2}^+[211])^2$.

[b] Excitation energy of level identified with configuration. Parentheses indicate tentative identification.

[c] Spectroscopic factors from Table V (ZRL, $N=4.42$). When it is possible for a transfer to proceed by two j values for the same l, tabulated S_{exp} corresponds to j that is predicted to have larger S. S_{exp} should then be compared with sum of the two S_{th} values for that l.

[d] Calculated using Eq. (3) and Woods-Saxon wave functions (Table IV and text).

[e] Impossible to separate 1.937- and 1.952-MeV states, however, $\sum_{l=2}(2J_f+1)S_{exp}=5.00$ compared with $\sum_{l=2}(2J_f=1)S_{th}=3.45$, 3.80, and 3.95 predicted, respectively, for $\delta=0.0$, 0.2625, and 0.525.

tion to be the 2^+ member of the $K=1$ rotational band based on the 1.937-MeV level. However, the $l=0$ spectroscopic factor observed for the 3.059-MeV 2^+ state is larger than that predicted at large deformations for the 2^+ member of this band. The 4.770-MeV level, whose (^{3}He, d) angular distribution is characteristic of pure $l=2$ (Fig. 4), may be the 3^+ member of this band. The observed spectroscopic factor for the 4.770-MeV level agrees well with the prediction for the 3^+ level for large deformations (Fig. 11). The observed spectroscopic factor for the known[16] 3^+ state at 2.969 MeV is also shown (Fig. 11) for comparison with the predicted spectroscopic factor for the 3^+ member of this $K=1$ rotational band.

The 2^+, 3^+, and 4^+ states of the $K=2$ band based on this same $\frac{3}{2}^+[211]$, $\frac{1}{2}^+[211]$ configuration should also be populated by the ^{21}Ne(^{3}He, d) reaction. In ^{22}Ne the levels identified[9] with the $K=1$ and 2 band heads of the $T=1$ part of this configuration (i.e., the states of ^{22}Ne at $E_x=5.36$ and 4.46 MeV, respectively) are separated by 0.9 MeV. If this same separation exists for the $T=0$ band heads, the 2^+ band head would then be located near 2.8 MeV. The predicted spectroscopic factors for the $K=2$ band head based on this configuration are also shown with the $l=0$ and 2 spectroscopic factors observed for the 2^+ level at 3.059 MeV (Fig. 11). The agreement (at large deformations) for the $l=0$ component is better for the $K=2$ band head than it is for the 2^+ state in the $K=1$ band. The $l=2$ spectroscopic factor, however, is in better agreement with the predictions based on the 2^+ state in the $K=1$ rotational band. The low-lying $J^\pi=2^+$, $T=0$ states will be discussed further in Sec. VI.

The level at 5.165 MeV has previously been suggested[1] to be the isobaric analog of the 2^+ state observed at 4.46 MeV in ^{22}Ne. The 4.46-MeV level in ^{22}Ne has been identified[9] as the $K=2$, $T=1$ band head based on the $\frac{3}{2}^+[211]$, $\frac{1}{2}^+[211]$ configuration. The observed spectroscopic factors for the level at 5.165 MeV in ^{22}Na are in good agreement (for deformations $\delta > 0.35$) with the predictions for the band head of the $K=2$, $T=1$ band based on this configuration (Fig. 11).

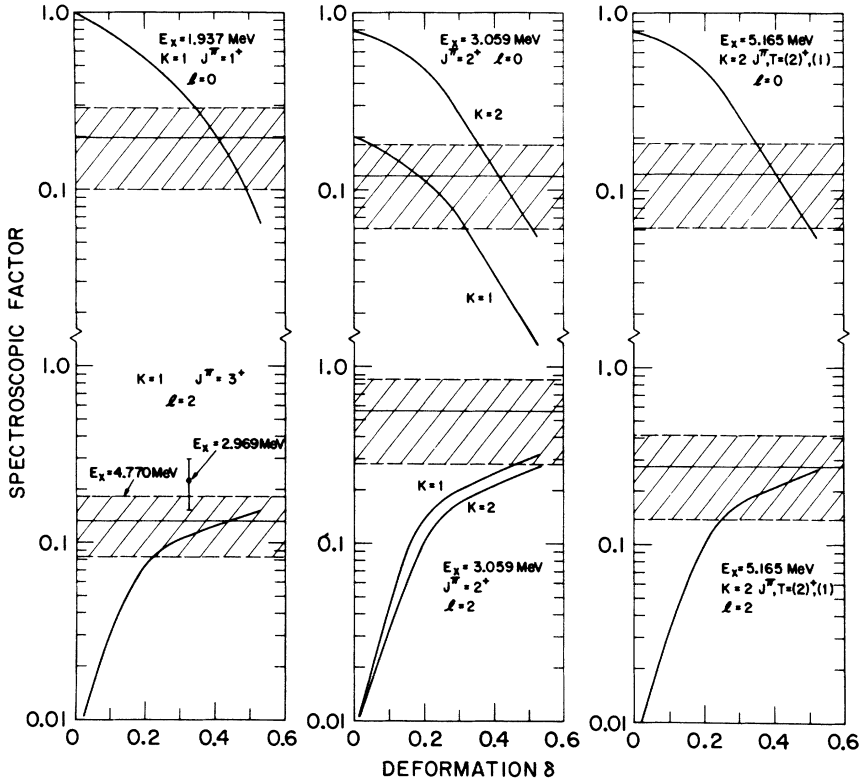

FIG. 11. Comparison of predicted and measured spectroscopic factors for states suggested as being based on the $\frac{3}{2}^+[211]$, $\frac{1}{2}^+[211]$ Nilsson configuration. The description is the same as Fig. 10. The experimental values for the 2^+ level at 3.059 MeV are compared with calculated values for the 2^+ states of both the $K=1$ and 2 rotational bands. Experimental values for the levels at 2.969 and 4.770 MeV are both compared with the predicted value for the 3^+ member of the $K=1$ band. See the text for a discussion of these levels.

C. States Based on Higher Positive-Parity Configurations

Another 1^+ state is observed at 3.944 MeV. The next predicted single-particle 1^+ state is a $K=1$ band head based on the $\frac{3}{2}^+[211]$, $\frac{5}{2}^+[202]$ configuration. Such a state would be populated by a pure $l=2$ (^{3}He, d) transition and is predicted for deformations of $\delta \approx 0.5$ to be about 2 MeV above the band heads based on the $\frac{3}{2}^+[211]$, $\frac{1}{2}^+[211]$ configuration. The 3.944-MeV level was observed to have a mixed $l=0+2$ (^{3}He, d) angular distribution (Fig. 3). The predicted $l=2$ spectroscopic factor for this level is independent of deformation and is observed to be larger than the experimental spectroscopic factor (Fig. 12). Its measured $l=0$ spectroscopic factor, $S_{exp}(0)(=0.10$; see Table V), is less than $S_{exp}(0)(=0.20)$ for the 1.937-MeV level but larger than $S_{exp}(0)(=0.04)$ for the 0.583-MeV level, which is also predicted to be excited by a pure $l=2$ transition. If the 3.944-MeV level is identified with the 1^+ member of the $\frac{3}{2}^+[211]$, $\frac{5}{2}^+[202]$ configuration, the configurations must be mixed, and the mixing is observed to increase with increasing excitation energy.

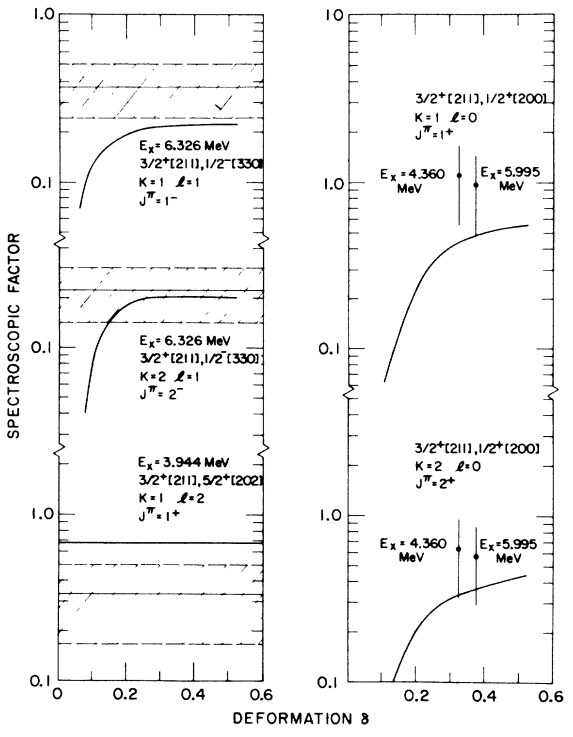

FIG. 12. Comparison of predicted and measured spectroscopic factors for additional states for which configurations can be suggested. The description is the same as Fig. 10. The $l=0$ experimental spectroscopic factors for the levels at 4.360 and 5 995 MeV are compared with the predicted values for both the $K=1$ and 2 bands based on the $\frac{3}{2}^+[211]$, $\frac{1}{2}^+[200]$ configuration. Similarly the $l=1$ experimental value is compared with predicted values for the $K=1$ and 2 negative-parity band heads based on adding a particle to the $\frac{1}{2}^-[330]$ Nilsson orbit. See the text for a discussion of these levels.

Based on the observed configuration mixing and the level density above 4.2 MeV, specific Nilsson configurations are not being proposed for most of the higher levels. However, two states, at 4.360 and 5.995 MeV, were observed to be populated with very strong $l=0$ transitions. The $K=1$ and 2 band heads based on the $\frac{3}{2}^+[211]$, $\frac{1}{2}^+[211]$ are predicted to have large $l=0$ spectroscopic factors for small deformations, whereas the $K=1$ and 2 band heads based on the $\frac{3}{2}^+[211]$, $\frac{1}{2}^+[200]$ configurations are predicted to have large $l=0$ spectroscopic factors for large deformations (Table VIII). Deformations are thought to be large, and the $K=1$ band head based on the $\frac{3}{2}^+[211]$, $\frac{1}{2}^+[211]$ configuration has already been tentatively identified with the level at 1.937 MeV. Thus the levels at 4.360 and 5.995 MeV are suggested to correspond to the $K=1$ and 2 band heads based on the $\frac{3}{2}^+[211]$, $\frac{1}{2}^+[200]$ configuration. The observed and predicted $l=0$ spectroscopic factors for these levels and configurations are compared in Fig. 12. A large $l=2$ spectroscopic factor is also observed for the level at 5.995 MeV. The simultaneously large $l=0$ and 2 spectroscopic factors can be accounted for in the simple model only if this level is a multiplet. Since spin 2(1) has previously been assigned to the level at 4.360 MeV,[16] this level is preferred as the $K=2$ band head.

D. States Based on Negative-Parity Configurations

A negative-parity band composed of states at (E_x in MeV, J^π) 2.211, 1^-; 2.572, 2^-; and 3.521, 3^- has previously been identified.[1, 2, 16] Deformations of order $\delta=0.5$ are required to explain negative-parity states this low in excitation (Fig. 9). For such deformations two Nilsson configurations may account for low-lying, negative-parity states: $\frac{3}{2}^+[211]$, $\frac{1}{2}^-[330]$ and $\frac{3}{2}^+[211]$, $\frac{1}{2}^-[101]$. For deformations of $\delta > 0.45$ the levels based on a particle in the $\frac{1}{2}^-[330]$ Nilsson orbital would be predicted to be lower in excitation than the $\frac{1}{2}^-[101]$ hole states. Such levels should be populated appreciably by the ^{21}Ne(^{3}He, d) reaction (Table VIII). The negative-parity states at 2.211, 2.572, and 3.521 MeV, however, were observed to be only weakly populated in this study ($S_{exp}=0.03$, 0.02, and <0.01, respectively). The states at 2.211 and 2.572 MeV are populated strongly in the ^{23}Na-(^{3}He, α) reaction.[42] Therefore, the dominant configuration of these states is most likely to be identified with the $K=1$ rotational band based on a

hole in the $\frac{1}{2}^-[101]$ Nilsson orbit.

The level at 6.326 MeV is the only level populated with sufficient $l=1$ (^{3}He, d) transition strength to be identified with adding a nucleon to the $\frac{1}{2}^-[330]$ Nilsson orbit. The spectroscopic factor observed for this level is compared (Fig. 12) with the predictions for both the $K=1$ and 2 band heads based on the $\frac{3}{2}^+[211]$, $\frac{1}{2}^-[303]$ configuration.

E. Comparison with the ^{21}Ne(d, p) Reaction

Table IX compares the spectroscopic factors observed[9] in the ^{21}Ne(d, p)^{22}Ne reaction at 12-MeV incident energy with the $T=1$ spectroscopic factors of this study. The spectroscopic factors are listed for all levels of ^{22}Ne below 6.5 MeV that were observed to have angular distributions characteristic of stripping. The agreement for the members of the ^{22}Ne ground-state band, the first three levels tabulated, is within the normal DWBA uncertainties. The $l=2$ spectroscopic factor for the (^{3}He, d) transition to the 5.165-MeV level in ^{22}Na is nearly two times the corresponding (d, p) spectroscopic factor. The strength of the (^{3}He, d) transition agrees better with the predicted strength (Table IX and Fig. 11).

The levels of ^{22}Ne observed at 5.33 and 5.36 MeV have been suggested[9] as the $J^\pi=2^+$ and 1^+ members of the $K=1$ rotational band based on the $\frac{3}{2}^+[211]$, $\frac{1}{2}^+[211]$ Nilsson configuration. The analogs of these states should appear with appreciable (^{3}He, d) strength near 6.00 MeV in ^{22}Na. A candidate would be the 5.995-MeV level in ^{22}Na with spectroscopic strengths $(2J_f+1)S_{exp}(0)=2.82$ and $(2J_f+1)S_{exp}(2)=3.98$. This level at 5.995 MeV, however, also was populated with appreciable strength by the ^{20}Ne(^{6}Li, α)^{22}Na reaction[1] and the ^{24}Mg(d, α)^{22}Na reaction,[17] both of which should populate only $T=0$ states. Thus the total strength of the 5.995-MeV level in ^{22}Na is not expected to be derived from the $T=1$ analogs of the 5.33- and 5.36-MeV ^{22}Ne levels. In the preceding subsection the 5.995-MeV level of ^{22}Na was identified with either the $K=1$ or 2 band head of the $T=0$ part of the $\frac{3}{2}^+[211]$, $\frac{1}{2}^+[200]$ configuration. This identification was based on the strong $l=0$ transition to this level. The experimental spectroscopic factors for the 5.995-MeV level are observed to be larger than those predicted for either of the $\frac{3}{2}^+[211]$, $\frac{1}{2}^+[200]$ configurations (Fig. 12). (This is especially true for the $l=2$ spectroscopic factor.) Since the total strength of the 5.995-MeV level can be accounted for by the Nilsson model only if it is a multiplet, this level probably consists of the assumed $T=0$ level and at least one of the $T=1$ levels expected in this excitation region. Based only on the (^{3}He, d)-(d, p) comparison, the level at 6.088 MeV in ^{22}Na [$(2J_f+1)S_{exp}(0)=0.72$ and $(2J_f+1)S_{exp}(2)=1.39$] could be one of the two $T=1$ states. Again, however, this level was populated in the ^{20}Ne(^{6}Li, α)^{22}Na and ^{24}Mg(d, α)^{22}Na studies.[1,17] Similarly, the 6.185-MeV level in ^{22}Na with $(2J_f+1)S(2)=6.18$ may also be a multiplet with one member being the analog of the 5.52-MeV ^{22}Ne level. This level was also excited by the ^{20}Ne(^{6}Li, α)^{22}Na and ^{24}Mg(d, α)^{22}Na reactions[1,17]; however, it was suggested as a probable doublet in the ^{24}Mg(d, α)^{22}Na and ^{23}Na(^{3}He, α)^{22}Na comparison.[17] To identify the $T=1$ states expected in the 5.9- to 6.2-MeV excitation region of ^{22}Na, additional ultrahigh resolution studies are needed.

F. Comparison with Shell-Model Calculations

Recently shell-model calculations have been per-

TABLE IX. Comparison of ^{21}Ne(^{3}He, d)^{22}Na and ^{21}Ne(d, p)^{22}Ne spectroscopic factors.

^{21}Ne(d, p)^{22}Ne [a]			^{21}Ne(^{3}He, d)^{22}Na [b]				
						Theory [c]	
E_x (MeV)	$(2J_f+1)S(0)$	$(2J_f+1)S(2)$	E_x (MeV)	$(2J_f+1)S(0)$	$(2J_f+1)S(2)$	$(2J_f+1)S(0)$	$(2J_f+1)S(2)$
g.s.	···	0.26 [d]	0.657	···	0.40	···	0.22
1.28	···	3.25	1.952	···	3.50 [e]	···	3.20
3.36	···	0.44	4.069	···	0.39	···	0.54
4.46	0.34	0.72 [d]	5.165	0.31	1.39	0.25 [f]	1.35
5.33	0.36	0.58					
5.36	1.56	···					
5.52	···	2.26					
5.64	···	0.49					

[a] See Ref. 9.

[b] Present work. S values based on $N=4.42$.

[c] Based on Eq. (3) and finite-well Nilsson wave functions for a deformation of $\delta=0.525$.

[d] Has been increased by 30% (Ref. 9) to account for DWBA calculation based on $j=\frac{3}{2}$ vice $j=\frac{5}{2}$.

[e] Calculated by subtracting predicted $(2J_f+1)S$ for 1.937-MeV level for $\delta=0.525$ from combined $(2J_f+1)S_{exp}$.

[f] Strong function of deformation; i.e., $(2J_f+1)S(0)=1.65$ for $\delta=0.2625$.

formed for up to six active nucleons in the $2s$-$1d$ shell.[46] The shell-model basis included all allowed states for the six active nucleons distributed among the $1d_{5/2}$, $2s_{1/2}$, and $1d_{3/2}$ subshells. Calculated excitation energies for the positive-parity states of ^{22}Na and predicted spectroscopic factors for the ^{21}Ne(^{3}He, d) reaction are compared with experimental values in Table X. The theoretical values tabulated are all based on the Kuo Hamiltonian[46,47] with single-particle energies taken[46] to be the neutron separation energies of the lowest $\frac{5}{2}^+$, $\frac{1}{2}^+$, and $\frac{3}{2}^+$ states in ^{17}O. Too many $T=0$, $J=2$, 3, and 4 states are predicted to occur below 4 MeV. The agreement of predicted and measured spectroscopic factors for the $T=1$ states and the $1_1 0$, $1_2 0$, $3_1 0$, and $4_1 0$ states is within the expected uncertainties. The agreement, however, is not as good for transitions to higher excited $T=0$ states, e.g., to the $1_3 0$, $1_4 0$, and $3_3 0$ states. The predicted spectroscopic factors of the rotational model agree better with the experimental values for the excited 3^+, $T=0$ states

TABLE X. Comparison with shell-model calculations.

	Experimental			Shell-model calculation [a]				
$J_i T$ [b]	E_x (MeV)	$S(l=2)$ [c]	$S(l=0)$ [c]	E_x (MeV)	$S(d_{5/2})$	$S(d_{3/2})$	$\sum S(l=2)$	$S(s_{1/2})$
$0_1 0$				5.41	···	0.52	0.52	···
$0_2 0$				8.25	···	0.37	0.37	···
$0_3 0$				10.30	···	0.00	0.00	···
$0_4 0$				12.92	···	0.00	0.00	···
$1_1 0$	0.583	0.65	0.04	−0.31	0.50	0.01	0.51	0.06
$1_2 0$	1.937	d	d	0.24	0.12	0.35	0.47	0.02
$1_3 0$	3.944	0.33	0.10	2.60	0.10	0.02	0.12	0.08
$1_4 0$	4.319	0.03	<0.01	4.48	0.01	0.18	0.19	e
$2_1 0$	3.059	0.56	0.12	0.77	0.08	0.26	0.34	0.07
$2_2 0$				1.99	0.02	0.20	0.22	0.07
$2_3 0$	(4.360)	~0.0	0.66	3.17	0.00	0.03	0.03	0.32
$2_4 0$				4.06	0.02	0.21	0.23	e
$3_1 0$	0.00	0.47	···	0.00	0.45	0.04	0.49	···
$3_2 0$	1.984	0.27	···	0.93	0.49	0.02	0.51	···
$3_3 0$	2.969	0.32		1.86	0.01	0.02	0.03	···
$3_4 0$				2.96	0.02	e	0.02	···
$4_1 0$	0.891	0.80	···	0.81	1.00	···	1.00	···
$4_2 0$				2.59	0.01	···	0.01	···
$4_3 0$				4.13	0.00	···	0.00	···
$4_4 0$				5.28	e	···	e	···
$0_1 1$	0.657	<0.40	···	0.00 [f]	···	0.11	0.11	···
$0_2 1$				4.95 [f]	···	0.04	0.04	···
$0_3 1$				6.81 [f]	···	0.00	0.00	···
$2_1 1$	1.952	d	d	1.14 [f]	···	···	0.89 [g]	0.01
$2_2 2$	5.165	0.28	0.12	3.53 [f]	···	···	0.26 [g]	0.25
$3_1 1$				4.51 [f]	···	···	0.33 [g]	···
$4_1 1$	4.069	0.04	···	3.21 [f]	0.05	···	0.05	···
$4_2 1$				5.54 [f]	0.00	···	0.00	···

[a] Calculations from Ref. 46 using $K+^{17}$O potential.

[b] $J_i T$ corresponds to ith state of spin and isospin J, T.

[c] Spectroscopic factors from Table V (ZRL, $N=4.42$). When it is possible for transfer to proceed by both $j=\frac{3}{2}$ and $\frac{5}{2}$ for $l=2$, the tabulated $S_{\exp}(l=2)$ corresponds to the j that is predicted to have the larger S. $S_{\exp}(l=2)$ should then be compared with the sum of $S_{\text{th}}(d_{5/2})$ and $S_{\text{th}}(d_{3/2})$, i.e., $\sum S(l=2)$.

[d] Impossible to separate 1.937- and 1.952-MeV states; however, $\sum(2J_f+1)S_{\exp}(l=2)=5.0$ and $\sum(2J_f+1)S_{\exp}(l=0)=0.58$, compared with $\sum(2J_f+1)S_{\text{th}}(l=2)=5.86$ and $\sum(2J_f+1)S_{\text{th}}(l=0)=0.11$.

[e] Not calculated (see Ref. 46).

[f] Excitation energies relative to lowest $T=1$ state which is observed experimentally at 0.657 MeV.

[g] Separate $j=\frac{3}{2}$ and $\frac{5}{2}$ spectroscopic factors not available. Tabulated value represents sum of spectroscopic factors for $j=\frac{3}{2}$ and $\frac{5}{2}$.

than do the shell-model predictions. Both rotational and shell models predict too many low-lying 2^+ states. Neither model can account for the (^{3}He, d) transition strength of the level at 3.059 MeV. It is interesting to note that the observed transition to this state is of sufficient strength to account for the sum strength of the predicted strength for $2_1 0$ and $2_2 0$.

VI. CONCLUSIONS

The agreement between the measured and the calculated spectroscopic factors for states based on the $(\frac{3}{2}^+[211])^2$ configuration is within the uncertainties of the DWBA calculations (Fig. 10). A small $l=0$ component, however, is observed in the (^{3}He, d) transition to the 0.583-MeV 1^+ state, whereas a pure $l=2$ transition is predicted by the Nilsson model (Table VIII).

TABLE XI. Possible explanations for the "missing" low-lying 2^+ state.

Configuration	K	J^π	Cases [a] I [b]	II [c]	III
$(\frac{3}{2}^+[211])^2$	0	3^+	2.969	1.984	1.984
$\frac{3}{2}^+[211]$, $\frac{1}{2}^+[211]$	1	2^+	1.984	2.969	3.059
$\frac{3}{2}^+[211]$, $\frac{1}{2}^+[211]$	1	3^+	4.770	4.770	2.969 or 4.770
$\frac{3}{2}^+[211]$, $\frac{1}{2}^+[211]$	2	2^+	3.059	3.059	>4.2

[a] Tabulated values are excitation energies of the level associated with the corresponding configuration K and J^π for that explanation.

[b] Case I assumes that the state at 1.984 MeV has been incorrectly assigned $J^\pi = 3^+$.

[c] Case II assumes that the state at 2.969 MeV has been incorrectly assigned $J^\pi = 3^+$.

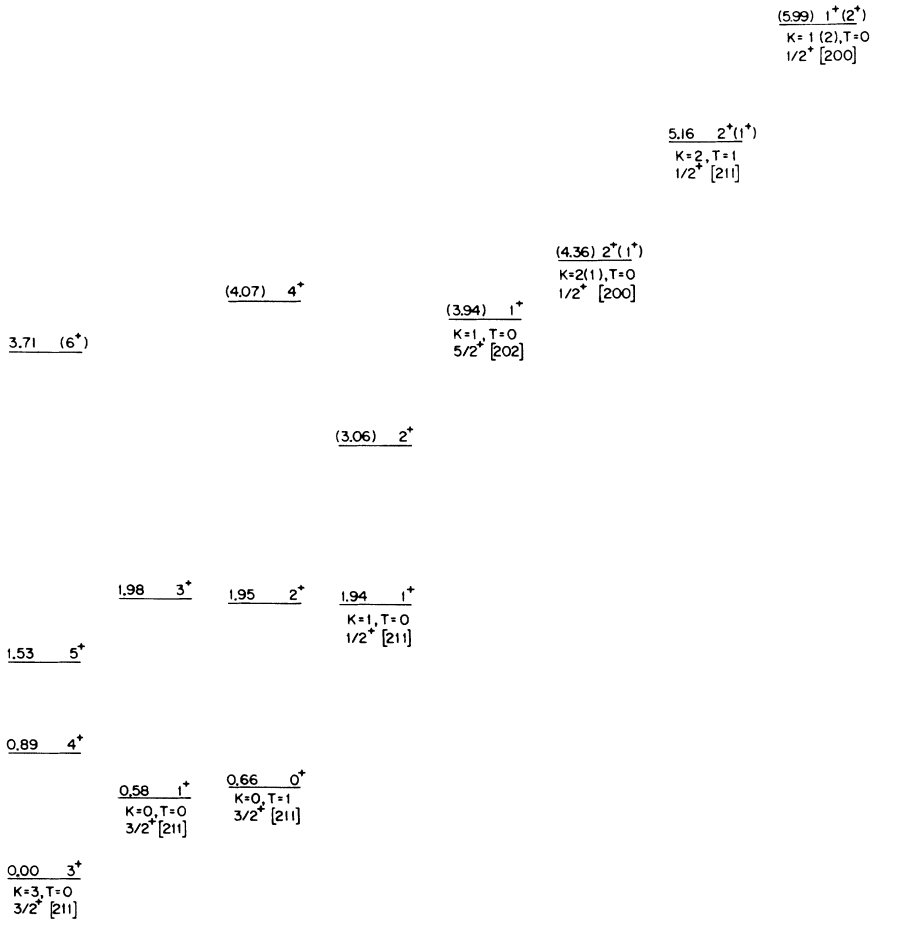

FIG. 13. Summary of positive-parity rotational bands in ^{22}Na. The assumed configuration of each band is a nucleon in the $\frac{3}{2}^+[211]$ Nilsson orbit coupled to a nucleon in the orbit listed for each band. Where an identification of an experimental state with a given configuration is considered tentative, its excitation energy is listed in parentheses. Not shown is the 3^+ member of the $K=1$, $T=0$ band based on the $\frac{3}{2}^+[211]$, $\frac{1}{2}^+[211]$ configuration since levels at 2.969 and 4.770 MeV are considered as equally likely choices (see Fig. 11 and text).

Since the levels of the negative-parity band based on the 1^- level at 2.211 MeV are excited only weakly in the ^{21}Ne(^{3}He, d) reaction but are populated strongly in the ^{23}Na(^{3}He, α) reaction,[42] they are identified as being predominantly based on the $\frac{3}{2}^+[211]$, $\frac{1}{2}^-[101]$ configuration. An additional negative-parity state at 6.326 MeV, that is populated strongly by the ^{21}Ne(^{3}He, d) reaction, is identified as either the $K=1$ or 2 band head of the $\frac{3}{2}^+[211]$, $\frac{1}{2}^-[330]$ configuration.

The 1^+ state at 1.937 MeV is suggested as being the $K=1$ band head based on the $\frac{3}{2}^+[211]$, $\frac{1}{2}^+[211]$ configuration even though such a state is predicted from the simple Nilsson model to lie above 4 MeV (Fig. 9). Two 2^+ states (the $K=2$ band head and the 2^+ level of the $K=1$ band based on the $\frac{3}{2}^+[211]$, $\frac{1}{2}^+[211]$ configuration) should be observed about 1 MeV above the 1^+ state at 1.937 MeV. Only one 2^+ $T=0$ state is observed below 4.2 MeV, and its experimental spectroscopic factors are greater than those predicted (at large deformations) for either of these 2^+ states based on the $\frac{3}{2}^+[211]$, $\frac{1}{2}^+[211]$ configuration. Three possible explanations exist for the 2^+ states of this configuration: (1) The state at 1.984 MeV has been wrongly assigned 3^+ and it is the second 2^+ state (the 3^+ state at 2.969 MeV would then be the 3^+ member of the $K=1$ band based on the 0.583-MeV level); (2) the 2.969-MeV level has been wrongly assigned 3^+, it being the missing 2^+ state; (3) the $K=2$ band head based on this configuration lies higher in excitation. These three possible alternatives are summarized in Table XI as cases I–III. Considering case I, the 1.984-MeV state has previously been suggested[31,48] as having spin-parity of 2^+. An apparent $L=4$ ^{20}Ne(^{3}He, p) transition[1] to this state, however, is inconsistent with spin 2. The 100% γ branch[20] from this state to the 1^+ state at 0.583 MeV [$|M(E2)|^2 = 25.3^{+6.8}_{-4.4}$ W.u. for $1.984 \rightarrow 0.583$[20] and $|M(E2)|^2 < 0.06$ W.u. for $1.984 \rightarrow 0.0$[2,20]] strongly suggests that this level is the 3^+ state of the $K=1$ band based on the 0.583-MeV 1^+ level. The 1.984-MeV level is populated strongly in the ^{23}Na(^{3}He, α) reaction, whereas the level at 2.969 MeV is not.[42] Assuming that the ground state of ^{23}Na is two neutrons and a proton in the $\frac{3}{2}^+[211]$ orbital with a completely paired ^{20}Ne core, states based on the $\frac{3}{2}^+[211]$, $\frac{1}{2}^+[211]$ configuration would not be populated by the ^{23}Na(^{3}He, α) reaction. States based on the $(\frac{3}{2}^+[211])^2$ configuration, however, would be populated by the pickup reaction. Hence the first explanation (case I of Table XI) can probably be ruled out. Considering the second explanation (case II), the level at 2.969 MeV was assigned spin 3 from γ correlation,[2,21] and lifetime[20] measurements and positive parity from a measurement of the linear polarization of the γ rays resulting from this state.[16] In the present study the level at 2.969 MeV was observed to be populated by a pure $l=2$ (^{3}He, d) transition (Fig. 4) which is consistent with its previous 3^+ assignment. An upper limit of $S_{\text{exp}}(l=0) \lesssim 0.015$ can be put on the $l=0$ transition to this level. A sizable $l=0$ transition is predicted for the missing $K=2$ band head. The theoretical $l=0$ transition, however, is smaller for transitions to the 2^+ member of the $K=1$ band at large deformations (Fig. 11). The final explanation (case III of Table XI) for the missing 2^+ state is that the $K=2$ band is much higher in excitation than the observed $K=1$ band [i.e., the $K=2$ band head is near where it is predicted by the simple Nilsson model (see Fig. 9) and the $K=1$ band has been depressed]. Mixing between the 2^+ members of the two bands may then help to account for the large observed spectroscopic factors for the 2^+ state at 3.059 MeV (Fig. 11) and the fact that the $K=1$ band is at a lower excitation than expected. If this explanation is accepted, two possibilities exist for the 3^+ member of the $K=1$ band: the 3^+ state at 2.969 MeV and the state at 4.770 MeV which is populated with a pure $l=2$ (^{3}He, d) transition (Fig. 4). The experimental spectroscopic factor for the level at 4.770 MeV is in better agreement with the predictions for the 3^+ member of this $K=1$ band (Fig. 11). If the state at 2.969 MeV is identified as the 3^+ member of the $K=1$ band, the excitation energies indicate that the band is strongly decoupled.

A 1^+ state at 3.944 MeV is tentatively identified as the $K=1$ band head of the $\frac{3}{2}^+[211]$, $\frac{5}{2}^+[202]$ configuration, even though a sizable $l=0$ transition (Fig. 3 and Table V) is observed to this state (the transition is predicted to be pure $l=2$). This identification is indicative of considerable mixing, in either the initial or final states which, furthermore, increases with increasing excitation. Because of this apparent mixing, we have refrained from further identification of positive-parity levels with specific configurations except for two levels (those at 4.360 and 5.995 MeV with the $\frac{3}{2}^+[211]$, $\frac{1}{2}^+[200]$ $T=0$ band heads) that were observed to be populated with very strong $l=0$ transitions.

The suggested positive-parity rotational bands in ^{22}Na are summarized in Fig. 13. Where an identification of an experimental state with a given Nilsson configuration is considered tentative, its excitation energy is listed in parentheses. The Nilsson configuration and K quantum number for each band is given below the band head.

ACKNOWLEDGMENTS

The authors are grateful to Dr. D. Kurath for discussions concerning the rotational-band sum

rules, to Dr. S. Wahlborn for performing the deformed Woods-Saxon calculations, and to Dr. Ole Hansen for discussions concerning their use. The authors are particularly indebted to P. Harduk for his assistance in designing the rotating gas target and for its construction. The authors also thank Mrs. M. Barnett for her careful scanning of the nuclear emulsions and Mrs. A. Garrett and Mrs. B. Pomerantz for their assistance in the data analysis.

---

*Work supported by the National Science Foundation.

[1]J. D. Garrett, R. Middleton, D. J. Pullen, S. A. Andersen, O. Nathan, and O. Hansen, Nucl. Phys. A164, 449 (1971).

[2]E. K. Warburton, A. R. Poletti, and J. W. Olness, Phys. Rev. 168, 1232 (1968).

[3]B. Hausser, B. Hooton, D. Pelte, T. Alexander, and H. Evans, Phys. Rev. Letters 22, 359 (1969).

[4]D. Schwalm and P. Povh, Phys. Letters 29B, 103 (1969).

[5]K. Nakai, F. Stephens, and R. Diamond, in *Proceedings of the International Conference on Properties of Nuclear States, Montréal, Canada, 1969,* edited by M. Harvey *et al.* (Les Presses de l'Université de Montréal, Montréal, Canada, 1969), p. 685.

[6]R. C. Bearse and J. L. Yntema, Phys. Rev. 175, 1442 (1968).

[7]J. Dubois, Nucl. Phys. A104, 657 (1967).

[8]J. M. Joyce, R. W. Zurmühle, and C. M. Fou, Nucl. Phys. A132, 629 (1969).

[9]P. Neogy, Ph.D. thesis, University of Pennsylvania, 1970 (unpublished); P. Neogy, W. Scholz, and R. Middleton, to be published.

[10]J. R. Powers, H. T. Fortune, O. Hansen, and R. Middleton, Bull. Am. Phys. Soc. 15, 484 (1970); and to be published.

[11]R. H. Siemssen, L. L. Lee, Jr., and D. Cline, Phys. Rev. 140, B1258 (1965).

[12]S. Nilsson, Kgl. Danske Videnskab. Selskab, Mat.– Fys. Medd. 29, No. 16 (1955).

[13]B. R. Mottelson and S. Nilsson, Kgl. Danske Videnskab. Selskab, Mat.– Fys. Medd. 1, No. 8 (1959).

[14]I. Kelson, Phys. Rev. 134, B267 (1964).

[15]J. Picard and A. G. De Pinho, Nuovo Cimento 41, 239 (1966).

[16]J. W. Olness, W. R. Harris, P. Paul, and E. K. Warburton, Phys. Rev. C 1, 958 (1970).

[17]S. Hinds, H. Marchant, and R. Middleton, Nucl. Phys. 51, 427 (1964).

[18]P. M. Endt and C. Van der Leun, Nucl. Phys. A105, 1 (1967).

[19]H. J. Maier, P. Pelte, J. G. Pronko, and C. Rolfs, Nucl. Phys. 84, 1 (1966).

[20]E. K. Warburton, J. W. Olness, and A. R. Poletti, Phys. Rev. 160, 938 (1967).

[21]A. R. Polleti, E. K. Warburton, J. W. Olness, and S. Hechtl, Phys. Rev. 162, 1040 (1967).

[22]A. R. Poletti, E. K. Warburton, and J. W. Olness, Phys. Rev. 164, 1479 (1967).

[23]J. G. Pronko, C. Rolfs, and H. J. Maier, Phys. Rev. 167, 1066 (1968).

[24]P. Paul, J. W. Olness, and E. K. Warburton, Phys. Rev. 173, 1063 (1968).

[25]E. K. Warburton, L. E. Carlson, G. T. Garvey, D. A. Hutchen, and K. P. Jacksen, Nucl. Phys. A136, 160 (1969).

[26]R. W. Kavanaugh, Bull. Am. Phys. Soc. 12, 913 (1967).

[27]A. E. Baugrund, A. Fischer, and A. Z. Schwarzschild, Nucl. Phys. A107, 411 (1968).

[28]K. W. Jones, A. Z. Schwarzschild, E. K. Warburton, and D. B. Fossan, Phys. Rev. 178, 1773 (1969).

[29]R. C. Haight, Ph.D. thesis, Princeton University, 1969 (unpublished).

[30]W. T. Vogelsang and J. N. McGruer, Phys. Rev. 109, 1663 (1958).

[31]T. Wei, Bull. Am. Phys. Soc. 12, 85 (1968); and as quoted in Haight, Ref. 29.

[32]H. H. Duhm, K. Peterseim, R. Seehars, R. Finlay, and C. Detraz, Nucl. Phys. A151, 579 (1970).

[33]J. D. Garrett, Ph.D. thesis, University of Pennsylvania, 1970 (unpublished).

[34]P. D. Kunz, University of Colorado Report No. COO-535-613 (unpublished).

[35]R. H. Bassel, R. M. Drisko, and G. R. Satchler, Oak Ridge National Laboratory Report No. ORNL-3240, 1962 (unpublished).

[36]J. D. Garrett, R. Middleton, and H. T. Fortune, Phys. Rev. C 2, 1243 (1970).

[37]P. J. A. Buttle and L. J. B. Goldfarb, Proc. Phys. Soc. (London) 83, 701 (1964).

[38]F. G. Perey and D. S. Saxon, Phys. Letters 10, 107 (1964).

[39]G. R. Satchler, Ann. Phys. (N.Y.) 3, 275 (1958).

[40]S. Wahlborn and G. Ehrling, to be published.

[41]B. Chi, Nucl. Phys. 83, 97 (1966).

[42]H. T. Fortune, J. D. Garrett, and R. Middleton, Bull. Am. Phys. Soc. 16, 36 (1971); J. D. Garrett, H. T. Fortune, and R. Middleton, to be published.

[43]J. D. Garrett, H. T. Fortune, and R. Middleton, Bull. Am. Phys. Soc. 16, 36 (1971).

[44]R. H. Bassel, Phys. Rev. 149, 791 (1966).

[45]J. P. Schiffer, in *Isospin in Nuclear Physics,* edited by D. H. Wilkinson (North-Holland Publishing Company, Amsterdam, The Netherlands, 1969), p. 665.

[46]E. C. Halbert, J. B. McGrory, B. H. Wildenthal, and S. P. Pandya, in *Advances in Nuclear Physics,* edited by M. Baranger and E. Vogt (Plenum Press, Inc., New York, 1970), Vol. 4.

[47]T. T. S. Kuo, Nucl. Phys. A103, 71 (1967).

[48]A. M. Baxter, B. W. J. Gillespie, and J. A. Kuehner, Can. J. Phys. 48, 2434 (1970).